

WRDC-TR-90-4066

AD-A227 709

# MODELING OF STRESSES IN COATED SOLIDS

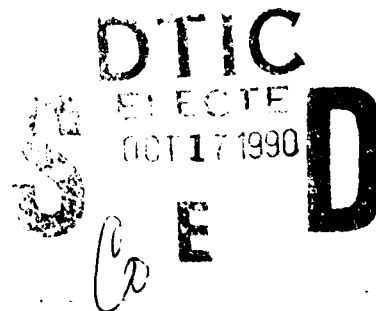


Pradeep K Gupta Inc  
117 Southbury Road  
Clifton Park, New York 12065

August 1990

Final Report for Period September 1989 - March 1990

Approved for public release; distribution unlimited



MATERIALS LABORATORY  
WRIGHT RESEARCH AND DEVELOPMENT CENTER  
AIR FORCE SYSTEMS COMMAND  
WRIGHT-PATTERSON AIR FORCE BASE, OHIO 45433-6533

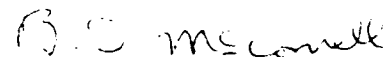
## NOTICE

WHEN GOVERNMENT DRAWINGS, SPECIFICATIONS, OR OTHER DATA ARE USED FOR ANY PURPOSE OTHER THAN IN CONNECTION WITH A DEFINITELY GOVERNMENT-RELATED PROCUREMENT, THE UNITED STATES GOVERNMENT INCURS NO RESPONSIBILITY OR ANY OBLIGATION WHATSOEVER. THE FACT THAT THE GOVERNMENT MAY HAVE FORMULATED OR IN ANY WAY SUPPLIED THE SAID DRAWINGS, SPECIFICATIONS, OR OTHER DATA, IS NOT TO BE REGARDED BY IMPLICATION, OR OTHERWISE IN ANY MANNER CONSTRUED, AS LICENSING THE HOLDER, OR ANY OTHER PERSON OR CORPORATION; OR AS CONVEYING ANY RIGHTS OR PERMISSION TO MANUFACTURE, USE, OR SELL ANY PATENTED INVENTION THAT MAY IN ANY WAY BE RELATED THERETO.

THIS REPORT HAS BEEN REVIEWED BY THE OFFICE OF PUBLIC AFFAIRS (ASD/PA) AND IS RELEASABLE TO THE NATIONAL TECHNICAL INFORMATION SERVICE (NTIS). AT NTIS IT WILL BE AVAILABLE TO THE GENERAL PUBLIC INCLUDING FOREIGN NATIONS.

THIS TECHNICAL REPORT HAS BEEN REVIEWED AND IS APPROVED FOR PUBLICATION.

  
SHASHI K. SHARMA, Project Engineer

  
B. D. McCONNELL, Chief  
Nonstructural Materials Branch

FOR THE COMMANDER

  
MERRILL L. MINGES, Director  
Nonmetallic Materials Division

IF YOUR ADDRESS HAS CHANGED, IF YOU WISH TO BE REMOVED FROM OUR MAILING LIST, OR IF THE ADDRESSEE IS NO LONGER EMPLOYED BY YOUR ORGANIZATION PLEASE NOTIFY WRDC/MLBT, WRIGHT-PATTERSON AFB, OH 45433-6533 TO HELP MAINTAIN A CURRENT MAILING LIST.

COPIES OF THIS REPORT SHOULD NOT BE RETURNED UNLESS RETURN IS REQUIRED BY SECURITY CONSIDERATIONS, CONTRACTUAL OBLIGATIONS, OR NOTICE ON A SPECIFIC DOCUMENT.

UNCLASSIFIED

SECURITY CLASSIFICATION OF THIS PAGE

REPORT DOCUMENTATION PAGE				Form Approved OMB No. 0704-0188	
1a. REPORT SECURITY CLASSIFICATION Unclassified			1b. RESTRICTIVE MARKINGS		
2a. SECURITY CLASSIFICATION AUTHORITY			3. DISTRIBUTION/AVAILABILITY OF REPORT Approved for Public Release; Distribution Unlimited		
2b. DECLASSIFICATION/DOWNGRADING SCHEDULE					
4. PERFORMING ORGANIZATION REPORT NUMBER(S)  G-110-TR			5. MONITORING ORGANIZATION REPORT NUMBER(S)  WRDC-TR-90-4066		
6a. NAME OF PERFORMING ORGANIZATION  Pradeep K Gupta Inc		6b. OFFICE SYMBOL (If applicable)	7a. NAME OF MONITORING ORGANIZATION Materials Laboratory (WRDC/MLBT) Wright Research and Development Center		
6c. ADDRESS (City, State, and ZIP Code) 117 Southbury Road Clifton Park, New York 12065			7b. ADDRESS (City, State, and ZIP Code) Wright-Patterson AFB, OH 45433-6533		
8a. NAME OF FUNDING/SPONSORING ORGANIZATION Materials Laboratory		8b. OFFICE SYMBOL (If applicable) WRDC/MLBT	9. PROCUREMENT INSTRUMENT IDENTIFICATION NUMBER  F33615-89-C-5648		
8c. ADDRESS (City, State, and ZIP Code) Materials Laboratory (AFSC) Wright-Patterson AFB, OH 45433-6533			10. SOURCE OF FUNDING NUMBERS		
			PROGRAM ELEMENT NO. 65502F	PROJECT NO. 3005	TASK NO. 52
11. TITLE (Include Security Classification)  MODELING OF STRESSES IN COATED SOLIDS					
12. PERSONAL AUTHOR(S) P. K. Gupta and J. A. Walowit (Consultant)					
13a. TYPE OF REPORT Final		13b. TIME COVERED FROM SEP89 TO MAR90		14. DATE OF REPORT (Year, Month, Day) 1990 August 06	
15. PAGE COUNT 71					
16. SUPPLEMENTARY NOTATION  Small Business Innovation Research Program - Phase I					
17. COSATI CODES			18. SUBJECT TERMS (Continue on reverse if necessary and identify by block number)		
FIELD	GROUP	SUB-GROUP	Coatings Composites Solid Lubricants		
			Coated Solids Composite Materials		
			Layered Solids Surface Films		
19. ABSTRACT (Continue on reverse if necessary and identify by block number)  A finite element approach to model stress distributions in coated solids is developed. The personal computer based PC-ANSYS code is used to implement the approach on a personal computer system. The three types of boundary loadign considered are an elliptical normal pressure distribution, a shear stress distribution proportional to the normal pressure, and a thermal flux proportional to the surface shear. The model predictions are validated against the classical Hertz theory and plane-strain solution obtained independently by well established Fourier transform approaches. The deviations of the finite element model from the other available solutions is found to be less than 1%. Parametric results of the model establish practical significance of the modeling approach for optimization of coating thickness, materials selection, and for the development of coating application techniques and procedures to ensure acceptable "break-away" stresses in the coating and at the coating/substrate interface. Extension of the finite element approach to the modeling of complex three-dimensional contacts is demonstrated by modeling a rectangular contact over					
20. DISTRIBUTION/AVAILABILITY OF ABSTRACT <input checked="" type="checkbox"/> UNCLASSIFIED//UNLIMITED <input type="checkbox"/> SAME AS RPT <input type="checkbox"/> DTIC USERS			21. ABSTRACT SECURITY CLASSIFICATION Unclassified		
22a. NAME OF RESPONSIBLE INDIVIDUAL SHASHI K. SHARMA			22b. TELEPHONE (Include Area Code) (513) 255-9029		22c. OFFICE SYMBOL WRDC/MLBT

Block 19 continued

a semi -infinite solid. This preliminary three-dimensional model, along with the two-dimensional parametric results demonstrate technical feasibility of the overall modeling approach. In addition, the results provide a strong analytical foundation for the development of a more rigorous and sophisticated models, and extended data bases for practical design of interacting coated solids for a wide range of practical applications.

## FOREWORD

This research was sponsored by the United States Air Force under the Defense Small Business Innovation Research (SBIR) Program, Air Force Contract Number F33615-89-C-5648. The Air Force Project Engineer was Mr. Shashi K. Sharma (WRDC/MLBT). The work reported herein constitutes Phase I effort of the overall program.



Accession For	
NTIS GRA&I	<b>X</b>
DTIC TAB	
Unannounced	
Justification	
By	
Distribution/	
Availability Codes	
Dist	Avail and/or Special
<b>A-1</b>	

## Table of Contents

<b>1.</b>	<b>INTRODUCTION</b>	<b>1</b>
<b>2.</b>	<b>ANALYTICAL APPROACH</b>	<b>3</b>
2.1	Finite Element Modeling	3
2.2	Numerical Integral Model	10
<b>3.</b>	<b>RESULTS</b>	<b>14</b>
3.1	Model Validation	14
3.2	Parametric Studies	20
3.3	Three Dimensional Finite Element Modeling	45
<b>4.</b>	<b>SUMMARY</b>	<b>53</b>
<b>5.</b>	<b>RECOMMENDATIONS FOR FUTURE DEVELOPMENT</b>	<b>55</b>
	<b>REFERENCES</b>	<b>57</b>
	<b>APPENDIX</b>	
	Thermal Analysis of Semi-infinite Solid with a Moving Heat Source	59

## 1. INTRODUCTION

The tribological behavior of the materials present at the interface between machine elements subjected to sliding interaction very often dominate the overall behavior and life of the entire mechanical system. Friction and wear of bearings, gears, cams and similar components, is a significant problem in a wide range of both DOD and commercial applications. The use of lubricating oils and greases is well known for reduction of friction and wear and as a result improvement in life of the overall mechanical system. However, these conventional lubricants can only perform satisfactorily in a limited range of operating temperatures. In the very high temperature environment of modern gas turbine applications, solid lubricants offer, perhaps, the only means of lubricating the interacting mechanical elements. Similarly at cryogenic temperatures, solid lubrication offers the only potential for reducing friction and wear between mating surfaces. Very often solid lubrication under the extreme operating environments is accomplished by applying one or more coatings of certain materials, which offer favorable tribological characteristics, to the mating surfaces. Quite often several thin coats of different materials may be used or certain composite materials may offer favorable friction and wear characteristics. The thermo-mechanical behavior of the coatings may vary from fully isotropic to highly anisotropic. In general, due to the greatly different constitutive behavior of the coatings compared to that of the substrate, an acceptable design of a coating-substrate system is dependent on realistic modeling of the stresses in the coatings in a prescribed operating environment. The stress distribution in the coating determines its mechanical survival; the tensile stresses in the coating are often responsible for fracture initiation while both the shear and tension at the coating/substrate interface affects the adhesion, or mechanical bond, of the coating to the substrate. A rigorous analytical modeling of these stresses as a function of materials properties and coating thickness is, therefore, essential. In addition to the prediction of optimum values of coating thickness for prescribed materials in a given operating environment, the models may be used to parametrically evaluate critical design parameters, such as shear and tensile stresses at the coating to substrate interface, thermal stresses induced by the difference in thermal coefficient of expansion between the coatings and substrate and realistic endurance limits when the coated elements are subjected to cyclic loading, to arrive at significant recommendations for the required materials for more advanced applications. The development of analytical models to compute the thermo-mechanical behavior of coated solids is, therefore, the primary objective of this project.

Due to a rather wide application potential, the analytical modeling of the contact mechanics and interfacial interactions in coated solids has been of significant interest in the recent years. In the past, both the solution to the contact problem and the stress distribution in the coating as a function of the prescribed boundary loading have been attempted. The solution to the contact pressure profile in the case of cylindrical contact between coated elastic solids has been obtained to varying degrees of sophistication by a number of investigators [1-8]. Most of the early work [1-5] considered an asymptotic problem of a very thin or thick coating. Meijers [5], while considering an elastic layer over a rigid substrate demonstrated that the solutions for a thin and thick layer overlap so well that these solution may apply to arbitrary layer thicknesses with excellent approximation. Wu, Chiu and Pao [6,7] considered the classical stress function approach to the contact problem of coated solids, and they clearly demonstrated

the mathematical complexity of the problem, particularly the numerical convergence problem as the material of the coating tends to become incompressible. Gupta and Walowit [8] resolved this problem by considering a Fourier transform of the Airy stress function and they obtained solutions where both the coating thickness and the coating to substrate modulus ratios may assume arbitrary values; in addition, they demonstrated that the Poisson's ratio may also be arbitrary and therefore, the incompressible materials may be properly modeled. In the area of stress distribution in the coating, most investigators considered either a uniform or an elliptical boundary loading. Lemcoe [9] considered a uniform pressure over the contact zone on a hard coating resting over a relatively soft substrate. Results for the stress distribution in the coating and substrate were presented for the cases when the coating is either in frictionless contact or bonded to the substrate. Barovich, et al. [10], used an elliptical pressure profile and obtained stress distribution when the ratio of modulus of elasticity of the coating to that of the substrate varied in the range of 0.25 to 4. Later Ku, et al. [11], considered surface shear and presented similar results for both elliptical and uniform shear prescribed at the coating surface. Based on the general solution to the contact problem [8], Gupta, Walowit and Finkin [12] considered an arbitrary pressure and shear loading on the coating surface, and they presented results for stress distribution in the coating, substrate and at the coating/substrate interface for a wide range of material properties. For practical designs, the work of Gupta and Walowit [8,12] has been implemented in a FORTRAN computer code, LAYER [13], which is presently operational on personal computer systems.

With particular emphasis on both DOD and commercial application, the models discussed above have several limitations; first, most of the models are restricted to a one coating system; second, essentially all of the modeling effort has been dedicated to the simulation of mechanical loadings and the thermal problem has been greatly neglected; finally, the modeling process has been restricted to fairly well defined plane strain contacts and application to real practical components with complex geometries, such as bearings and gears, has been restricted. Since, on tribological grounds, there is a definite potential for the use of multicoated configurations and substantial thermal gradients are often present, refinements of the current models to help eliminate both these restrictions are essential for the development of viable analytical tools. In addition, analytical techniques for developing realistic solutions for complex geometries and simulations of three-dimensional contacts are essential for the performance predictions of practical components. The recent advancements in finite element methods offer substantial potential in this area. The finite element algorithms permit modeling of all geometrical and thermal effects. However, before the model can be used for practical design, validation against other numerical solutions and experimental data is essential. An advancement of the current models for plane strain contacts and the initial formulation for a finite element model are, therefore, the objective of Phase I of the proposed project. The technical feasibility of the finite element approach is proven by validating the solutions obtained under plane strain conditions against similar solutions obtained by other proven numerical techniques for such simplified contact geometries. In addition, the practical significance of the modeling approach is demonstrated by parametric computer runs which show the variation of stresses as a function of material properties and coating thickness. Thus, the overall feasibility of the modeling approach for materials selection and practical design in a given operating environment is demonstrated.



## 2. ANALYTICAL APPROACH

The contact problem of a coated solid is shown schematically in figure 2-1, where a coating of finite thickness is applied to a semi-infinite substrate. Under simplified plane strain conditions, such a configuration could simulate either a pure rolling contact, or a combined rolling-sliding contact as would occur in rolling element bearings, gears or cams. The elliptical loading, shown in the figure, may have three components: normal loading, shear loading and thermal loading. For normal loading, the pressure distribution  $p(x)$ , for a Hertzian line contact is given by the relationship

$$p(x) = p_h \left[ 1 - \left( \frac{x}{a} \right)^2 \right]^{1/2} \quad (1)$$

where  $p_h$  is the maximum Hertz pressure and  $a$  is the contact half width.

The surface shear loading  $\tau(x)$ , corresponding to a prescribed friction or traction coefficient,  $\mu$ , may be written as a product of the normal contact pressure and the traction coefficient

$$\tau(x) = \mu p(x) \quad (2)$$

If the slip rate between the two interacting surfaces is  $u$ , then the thermal loading would arise from the flux,  $\varphi$ , dissipated into the coated surface, which is given by the relationship

$$\varphi(x) = \beta \mu u p(x) \quad (3)$$

where  $\beta$  is fraction of heat transferred to the coated surface under consideration while the remainder goes to the other surface.

Using the above three types of general loading, two different analytical approaches are considered: a finite element approach which permits modeling of any geometry and a Fourier transform approach which provides numerically accurate solutions for a simplified contact geometry. With the ultimate objective of developing viable design tools for a wide range of practical applications, the technical feasibility of finite element approach is demonstrated by validation of the finite element solutions against corresponding solutions obtained by the Fourier transform approach and the classical Hertz contact theory. The highlights of both approaches are briefly discussed below.

### 2.1 Finite Element Modeling

The two of the most commonly available finite element codes are NASTRAN and

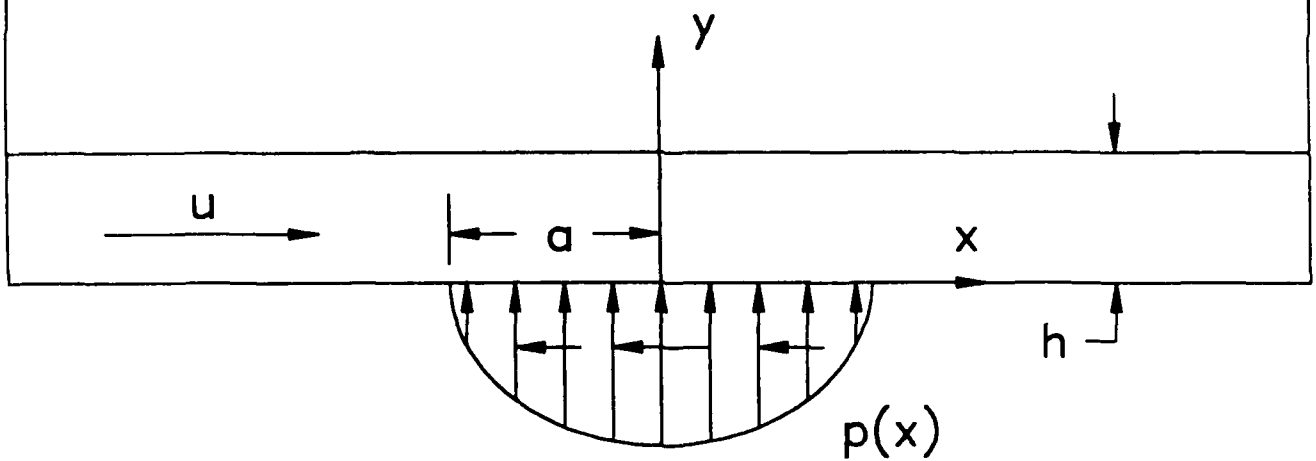


Figure 2-1. Coordinates for stress analysis in coated solid.

ANSYS. Both of these packages have the capability of modeling all three types of loading discussed above. However, ANSYS is readily available for personal computers, and its interactive user interfaces are, perhaps, more developed for efficient solutions of a wide range of problems on a personal computer. Due to such a readily available capability, the PC-ANSYS is selected for the present investigation, although the personal computers are still limited in terms of overall computing power required for sophisticated finite element modeling. Once the overall technical feasibility of the finite element approach is proven in the present Phase I effort, a more rigorous modeling shall be undertaken in the second phase of this project. In fact, as will be discussed later, the use of NASTRAN may be more appropriate in Phase II, since it is presently supported on the ASD computer system at Wright-Patterson Air Force Base. The transition from PC to main frame, or even from ANSYS to NASTRAN is indeed quite straightforward.

Similar to NASTRAN, ANSYS runs in three stages: a preprocessor, the main processor and a postprocessor. The preprocessor generates an input file for the main processor which, in turn, generates the stiffness matrices, computes element solutions and generates a binary output file for postprocessing. The postprocessor takes the output file and generates ASCII text and graphical outputs.

For the present problem, the element type and geometry, material properties and the mechanical and thermal loading parameters are all input via the preprocessor. Although the normal loading can be specified directly in terms of the prescribed contact pressures, the shear loading needs to be input in terms of forces at each node on the surface. In addition, the thermal loading is input in terms of a temperature field. The temperatures at each of the nodes are generated from a finite difference analysis, described in the Appendix. To prescribe all these inputs efficiently a personal computer based "pre-preprocessor" program has been written. This program generates the grid points (either automatically or from the optional user supplied data), computes temperatures at each point, computes normal and shear nodal forces on the surface and transmits all the data to input file as required by the ANSYS preprocessor. Installation of this input data preparation program to the main frame computer system, in Phase II, is quite straightforward.

Similar to the input data preparation effort, some analysis of the output from the ANSYS postprocessor is required for efficient handling of the output data. Thus a "post-postprocessor" is written to provide some degree of database management of multiple ANSYS output files, provide means for superposition of stresses obtained from various solutions, enable extended data reduction in the form of additional dimensionless quantities, provide improved output quality with convenient units and smoothing, and finally to obtain usable hard copy. Again, transfer of this procedure for use on main frame computer system, in Phase II, can be very easily carried out.

### **2.1.1 Element Generation Procedure**

The type of element geometry used is shown in figure 2-2. The normal Hertzian loading in the contact zone is shown by arrows. To accurately represent a semi-infinite geometry to compare the solutions with those obtained from the Hertzian theory, the geometry used

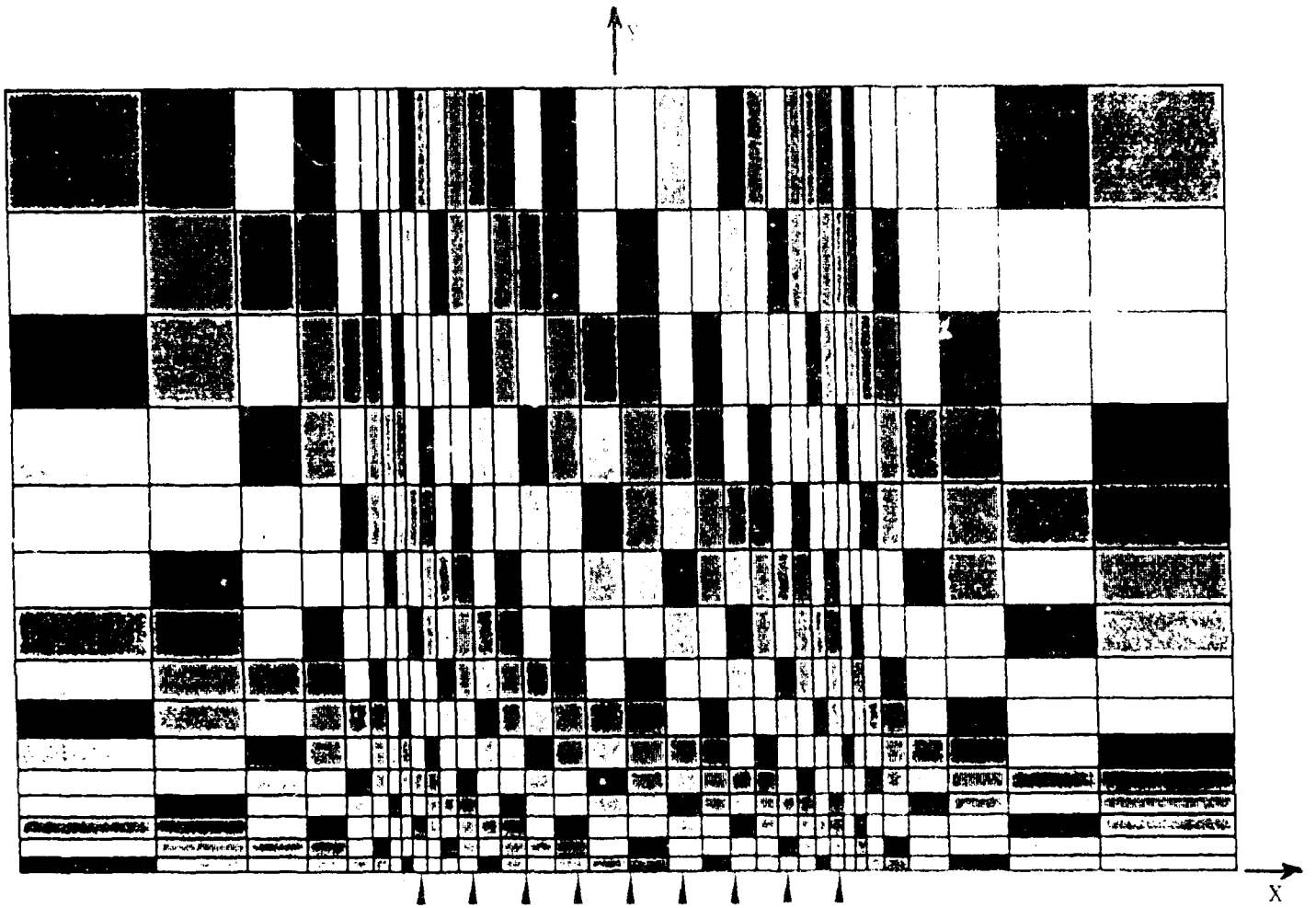


Figure 2-2. Finite element grid schematic.

extends 100 half widths in the positive and negative  $x$  and  $y$  directions.

Four node isoparametric elements with two degrees of freedom at each node are used in all two dimensional models. In order to capture rapid variations and produce accurate solutions, very fine mesh sizes are required in the  $y$  direction near the surface and near the coating to substrate interface. Also, due to the elliptical variation of surface loading, fine mesh sizes are needed near the edges of the contact. The method of mesh generation is illustrated in figure 2-3 which presents an enlarged view of the element geometry near the contact zone. The minimum mesh size, location of the outer boundaries, and the number of grid points in each direction are taken as inputs. Values for these quantities are dictated by trade-offs between overall accuracy, available storage and computing speed. In the absence of a coating, the minimum mesh size in  $y$  direction is used at the surface. An appropriate ratio,  $r$ , is calculated so that the length of each successive element in the  $y$  is  $r$  times that of the preceding element and the outer boundary is reached at the prescribed number of mesh points. A similar procedure is used for  $x$  direction. The  $x$  grid is taken to be symmetric about the center of contact. The prescribed minimum grid size in the  $x$  direction is used at the edge of contact. The number of elements between the center and edge of contact, and between the edge and outer boundary, are equal. Appropriate  $r$  values are calculated for each region.

A similar procedure is used for grid selection in the  $x$  direction when a coating is present. Initially, the procedure described above to calculate the  $r$  values in  $y$  direction is also used in the presence of a coating. The minimum grid size is then adjusted such that the grid line, which was initially the first line past location of the coating, falls directly on the coating location. The same  $r$  value is then used with the remaining number of points to generate the grid between the coating and the outer boundary. Finally, two additional grid lines are inserted at a distance equal to the prescribed minimum grid size on each side of the coating. The grid generated in this manner is shown schematically in figure 2-4.

The above procedure for grid generation assures relatively high accuracy with a given number of grid points in a rectangular region.

### **2.1.2 Inputs to the Finite Element Model**

Aside from the various thermal parameters outlined in the Appendix, the elastic modulus, Poisson's ratio and the thermal coefficient of expansion are required for both the coating and substrate material. As an example, the data shown in table 2-1, are used to generate finite element solutions at varying values of coating thickness. The thermal partition parameter,  $\beta$ , as discussed above is assumed to be unity, which means that the entire heat generated on the surface is transmitted into the coated solid. This may, indeed, be a conservative assumption. All the linear dimensions and stresses are respectively scaled relative to the contact half width,  $a$ , and the Hertzian contact pressure,  $p_h$ .

Solutions are obtained with both normal and shear loading on the surface. An elliptical distribution, conforming to equation (2-1) is used for both types of loadings. Also, the thermal flux is also assumed to be elliptical in accordance with equation (2-3).

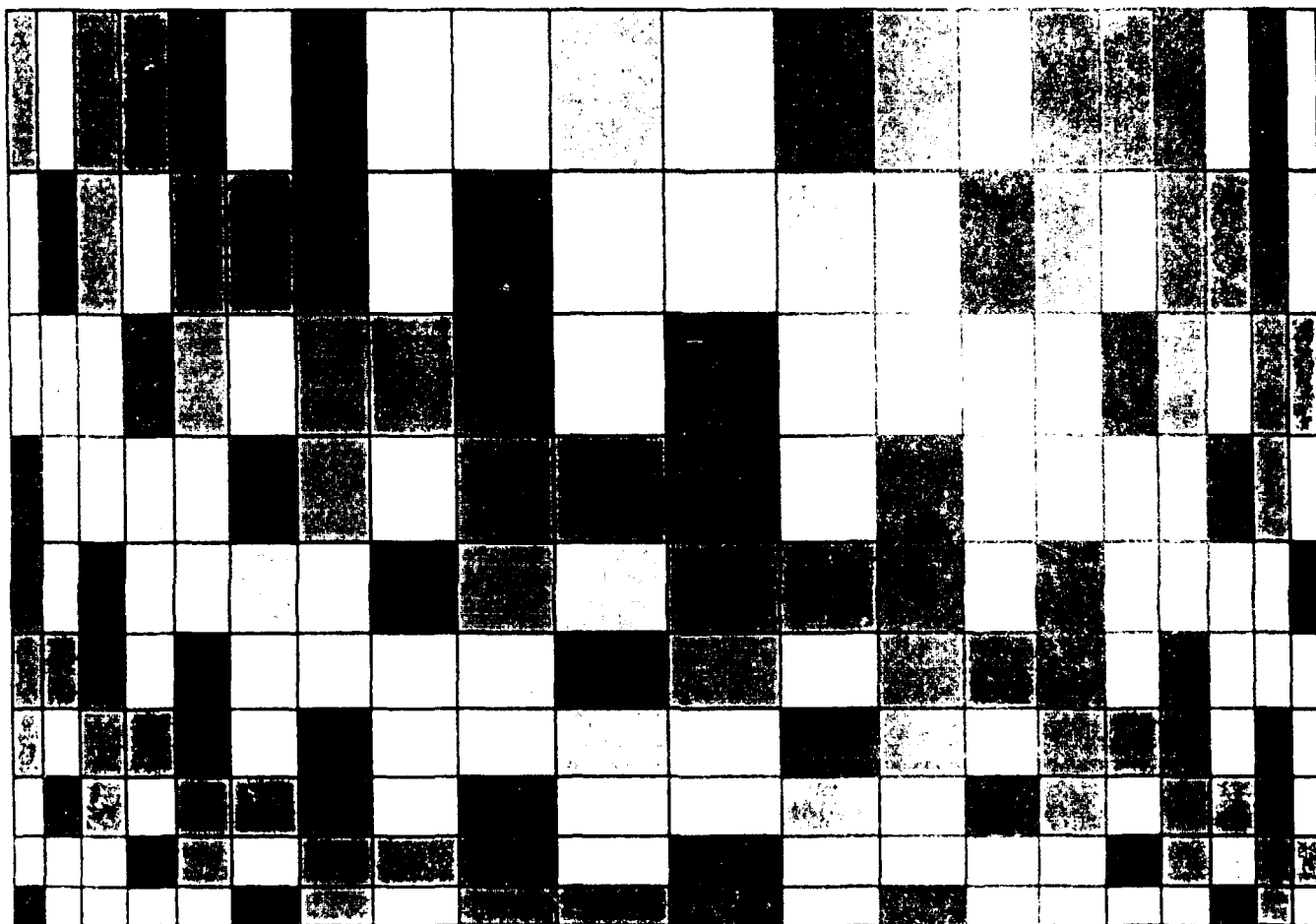


Figure 2-3. Grid structure near the contact with  $\alpha = 0.01$ .

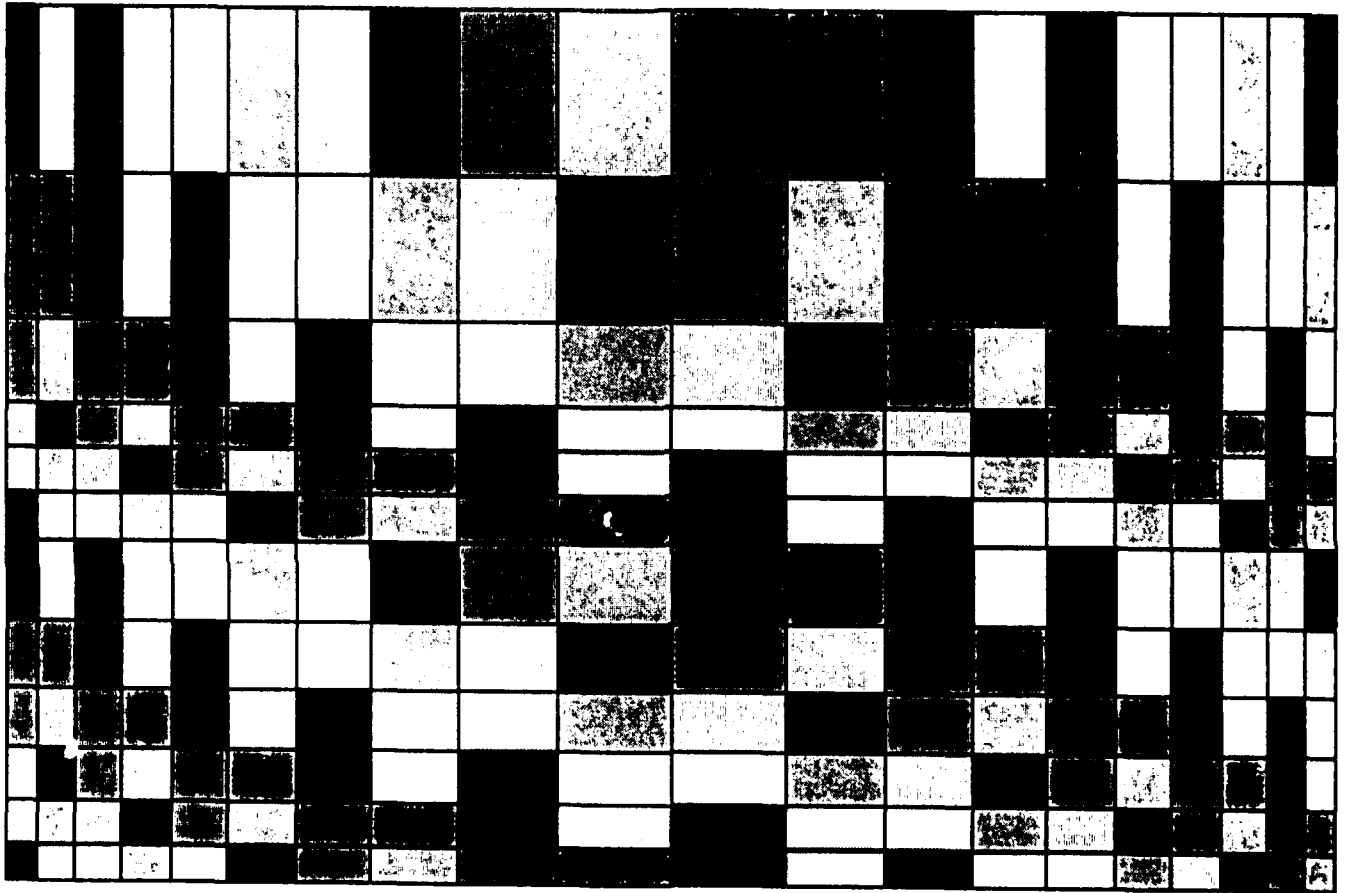


Figure 2-4. Grid structure near the contact with coating.

In addition to the above parameters, the following two boundary conditions, prescribed with reference to the coordinate frame shown in figure 2-1, complete the input data to the finite element model:

1. The force on the coating surface outside the contact region ( $y=0$ ,  $|x| > a$ ), and at the ends ( $|x| = 100a$ ), is zero.

2. Deflection is zero at all distant points ( $y=100a$ ).

**Table 2-1**  
**Input Values Used in Finite Element Analysis**

Symbol	Description	Value
$p_h$	Maximum Hertz pressure (Pa)	$1.0 \times 10^9$
$\mu$	Traction coefficient	1*
$E_1$	Coating elastic modulus (Pa)	$4.0 \times 10^{11}$
$E_2$	Substrate elastic modulus (Pa)	$2.0 \times 10^{11}$
$\nu_1$	Coating Poisson's ratio	0.3
$\nu_2$	Substrate Poisson's ratio	0.3
$\alpha_1$	Coating thermal coefficient expansion ( $^{\circ}C$ )	$2.78 \times 10^{-6}$
$\alpha_2$	Substrate thermal coefficient expansion ( $^{\circ}C$ )	$5.56 \times 10^{-6}$
$P$	Peclet number	100
$N$	Nusselt number	0
$T_r$	Reference loading temperature ( $^{\circ}C$ )	50
$T_a$	Ambient temperature ( $^{\circ}C$ )	20
$K_1/K_2$	Conductivity ratio	1
$K_1 \rho_2 c_2 / K_2 \rho_1 c_1$	Diffusivity ratio	1

\* For the results to be applicable to any value of traction, they are generated with a unit coefficient. Thus the results obtained with surface shear may be multiplied with appropriate traction coefficient when applying them to a specific contact.

## 2.2 Numerical Integral Model

An alternative numerical approach to compute the stresses in a coated solid is based on the work by Gupta and Walowit [8] and Gupta et al. [12]. The approach is primarily based



on a plane strain formulation derived from the Fourier transform of the classical Airy stress function. With reference to the coordinate frame shown in figure 2-1, the stresses  $\sigma_x$ ,  $\sigma_y$ , and  $\tau_{xy}$ , are respectively given by the relations:

$$\sigma_x = \frac{\partial^2 \psi}{\partial y^2} = \frac{1}{2\pi} \int_{-\infty}^{\infty} \frac{d^2 G}{dy^2} e^{-i\omega x} d\omega \quad (2-4)$$

$$\sigma_y = \frac{\partial^2 \psi}{\partial x^2} = -\frac{1}{2\pi} \int_{-\infty}^{\infty} \omega^2 G e^{-i\omega x} d\omega \quad (2-5)$$

$$\tau_{xy} = -\frac{\partial^2 \psi}{\partial x \partial y} = \frac{1}{2\pi} \int_{-\infty}^{\infty} i\omega \frac{dG}{dy} e^{-i\omega x} d\omega \quad (2-6)$$

where  $\psi$  is the Airy stress function which satisfies the biharmonic equation and  $G$  is the Fourier transform of  $\psi$ , symbolically,

$$\nabla^4 \psi = 0 \quad (2-7)$$

and

$$G = \int_{-\infty}^{\infty} \psi e^{i\omega x} dx \quad (2-8)$$

Also, the normal strains,  $\epsilon_x$  and  $\epsilon_y$ , and the displacements,  $u$  and  $v$ , along the  $x$  and  $y$  direction are given by

$$\epsilon_x = \frac{1}{E} \left[ (1 - \nu^2) \sigma_x - \nu (1 + \nu) \sigma_y \right] \quad (2-9)$$

$$\epsilon_y = \frac{1}{E} \left[ (1 - \nu^2) \sigma_y - \nu (1 + \nu) \sigma_x \right] \quad (2-10)$$

$$u = \frac{1 - \nu^2}{2\pi E} \int_{-\infty}^{\infty} \left[ \frac{d^2 G}{dy^2} + \left( \frac{\nu}{1 - \nu} \right) \omega^2 G \right] i e^{-i\omega y} \frac{d\omega}{\omega} \quad (2-11)$$

$$\nu = \frac{1-\nu^2}{2\pi E} \int_{-\infty}^{\infty} \left[ \frac{d^3 G}{dy^3} - \left( \frac{2-\nu}{1-\nu} \right) \omega^2 \frac{dG}{dy} \right] i e^{-i\omega y} \frac{d\omega}{\omega} \quad (2-12)$$

where  $E$  is the elastic modulus and  $\nu$  is the Poisson's ratio.

By eliminating  $\psi$  in equations (2-7) and (2-8), and by solving the resulting differential equation in  $G$ , the general solution may be shown to be of the form

$$G = (A + By) e^{-|\omega|y} + (C + Dy) e^{+|\omega|y} \quad (2-13)$$

where  $A$ ,  $B$ ,  $C$  and  $D$  may, in general be functions of  $\omega$  and they are determined by appropriate boundary conditions.

In the absence of any thermal effects or temperature fields, the boundary conditions for the coating/substrate system, as shown schematically in figure 2-1, may be readily expressed as

$$(\sigma_{y1})_{y_1=0} = -p(x) \quad (2-14a)$$

$$(\tau_{xy1})_{y_1=0} = q(x) \quad (2-14b)$$

$$(\sigma_{y1})_{y_1=h} = (\sigma_{y2})_{y_2=0} \quad (2-14c)$$

$$(\tau_{xy1})_{y_1=h} = (\tau_{xy2})_{y_2=0} \quad (2-14d)$$

$$(u_1)_{y_1=h} = (u_2)_{y_2=0} \quad (2-14e)$$

$$(\nu_1)_{y_1=h} = (\nu_2)_{y_2=0} \quad (2-14f)$$

$$(\sigma_{y2})_{y_2=\infty} = 0 \quad (2-14g)$$

$$\left( \epsilon_{xy2} \right)_{y2 = \infty} = 0 \quad (2-14h)$$

where the subscripts 1 and 2 denote the coating and substrate respectively. The variables  $y_1$  and  $y_2$  are measured respectively from the coating surface and the coating/substrate interface.

The above eight boundary conditions result in eight simultaneous algebraic equations for the coefficients  $A_1, B_1, C_1, D_1, A_2, B_2, C_2, D_2$ . Obviously conditions (2-14g) and (2-14h) result in  $C_2 = D_2 = 0$ . The remaining six algebraic equations are easily solvable for prescribed surface pressure,  $p(x)$ , and surface shear,  $q(x)$ .

Although when the coating is bonded to the substrate the strains are always continuous at the interface, the influence of different thermal coefficient of expansion is modeled, as a first approximation, in terms of a discontinuous strain boundary condition. Thus for a temperature rise,  $T$ , at the coating/substrate interface, the boundary condition (2-14f) is replaced by

$$\left( \epsilon_{x1} \right)_{y1 = h} - \left( \epsilon_{x2} \right)_{y2 = 0} = (\alpha_1 - \alpha_2) T \quad (2-15)$$

where  $\alpha_1$  and  $\alpha_2$  are the thermal coefficient of expansion respectively for the coating and substrate, and  $T$  is the temperature rise above nominal conditions.

In the absence of a rigorous thermal analysis, we further assume that the temperature profile at the coating/substrate interface is proportional to the contact pressure at the coating surface. Thus, for any prescribed maximum temperature in the contact, the required temperature profile is computed from the given pressure distribution at the coating surface.

Based on the above analytical formulation, the available computer code LAYER is modified for the thermal boundary condition (2-15). Such a modified version provides results to assess the significance of the thermal mismatch in properties of the coating and substrate. A more detailed analysis shall be undertaken in the second phase of this project, where a detailed temperature field, as presently computed for the finite element, shall be incorporated in the numerical integral solution model.

To compare the results from the finite element model with those obtained with the above numerical formulation, parametric runs are made with identical material properties and coating thickness. In addition, some parametric runs are made as a function of varying material properties, coating thicknesses and operating temperatures to establish the practical design significance of the overall modeling approach.

### 3. RESULTS

In order to validate the finite element model, the first set of results are obtained without any surface coating. These solutions may be compared directly with those obtained by the classical Hertz theory. In fact, comparison of the results obtained by both the finite element and Fourier transform approach with the Hertz solutions strengthens the practical significance of both models. Once these fundamental validations are made, the results obtained with coated solids with both models are then compared. Finally, some parametric results are obtained to prove the overall technical feasibility and establish the significance of the modeling approach for practical design and materials selection.

#### 3.1 Model Validation

In the absence of any surface coating and with an elliptical pressure distribution on the surface, numerical solutions for the stresses,  $\sigma_x$  and  $\sigma_y$ , as a function of the depth coordinate ( $y$  axis) are compared with the corresponding Hertz solutions in table 3-1; note that  $\sigma_h$ , in all the tables presented below, is the Hertzian contact pressure  $-p_h$ . Clearly, the finite element solutions and the predictions of the Fourier transform model are very close to the Hertz solution. In fact, the maximum deviation from the Hertz solutions is approximately 1%. This deviation can be further reduced by refining the mesh size and moving the distant boundary farther than the present value of 100 times the half width while setting up the finite element model. Some of these refinements greatly increase the mass storage and computing time requirements, which impose some restrictions on use of the model on a personal computer system. The use of a main frame computer system will certainly help in this regard. For most practical purposes, however, a deviation of about 1% is quite acceptable, and the model, in its present form, has reasonable design significance.

**Table 3-1**  
**Comparisons with Hertz Solutions**

$\frac{y}{a}$	Hertz Solution		Finite Element Solution		Fourier Solution	
	$\sigma_x/\sigma_h$	$\sigma_y/\sigma_h$	$\sigma_x/\sigma_h$	$\sigma_y/\sigma_h$	$\sigma_x/\sigma_h$	$\sigma_y/\sigma_h$
0.0091127	0.981899	0.999958	0.9719	1.000	0.9761	0.9916
0.09988	0.815139	0.995049	0.8043	0.9958	0.8163	0.9916
0.26875	0.567735	0.965732	0.5566	0.9655	0.5679	0.9655
0.57351	0.291086	0.867464	0.2811	0.8661	0.2911	0.8675
0.8334	0.168499	0.768189	0.1600	0.7672	0.1685	0.7682
1.0000	0.121320	0.707107	0.1131	0.7054	0.1213	0.7071
2.1054	0.0218005	0.429034	0.01548	0.4290	0.02180	0.4290

Similar to the finite element model, the grid size and the upper limits of integration used while performing a Fourier transform, may further improve the accuracy of the predicted results. For practical purposes, once again, the results are quite acceptable since the deviation is no more than 1%.

Perhaps the most interesting case for validation of the finite element model is to compare the stress  $\sigma_x$ , on the surface as generated by a shear loading. With the selected mesh size, it is confirmed that the deviation of the numerical results from the Hertzian solutions is within the above 1% limit. The comparison is shown graphically in figure 3-1, where the marked points represent finite element solution and the solid line represents the Hertz theory. The corresponding comparisons of the shear stress as a function of depth are shown in figure 3-2. Again, the model predictions are quite acceptable.

Another set of results is obtained with coated solids with both the finite element and Fourier transform approach. For a normal elliptical pressure loading on the surface, comparison of predicted stresses versus depth at  $x = 0$ , by the two models are shown in tables 3-2 and 3-3 respectively for the coating thickness to contact half width ratios ( $a/h$ ) of 0.25 and 0.50. Clearly, the solutions are very close to each other. In fact, the deviation is of the same general order as that seen above while comparing the solutions with the Hertz theory.

For an applied elliptical shear loading on the coating surface, the predicted distribution of shear stress, at  $x = 0$ , as a function of depth by the two models are compared in tables 3-4 and 3-5. Once again, the deviations between the two solutions are quite small, and both models are in good agreement with each other.

The above results clearly prove the validity of both models. Both the finite element or the Fourier transform approach provide acceptable prediction of stresses in coated solids. In terms of actual implementation for practical design, the finite element model can be effectively used for arbitrarily complex geometries, while the integral formulation is limited to simplified contact configurations. On the other hand, the finite element models require some effort in the pre and postprocessing of the data and overall setup of the problem, while the use of the numerical integral model is very straightforward. Thus depending on complexity of the application, both models may have a notable practical significance. For material selection and preliminary design, the Fourier transform approach may be very efficient, while for final design development for critical and complex applications, the finite element approach may provide acceptable design solutions with minimum number of model assumptions and limitation. For a more "friendly" implementation, both models may be run over a wide range of contact configurations and material properties, and a design data base may be generated to catalog these solutions over a wide range of applications. For a specific design, the data base can then provide very quick and accurate answers to a range of practical problems. The strengths of the models in generating such a data base is demonstrated by the parametric runs discussed next.

# FEM SOLUTION VS. HERTZ CONTACT THEORY

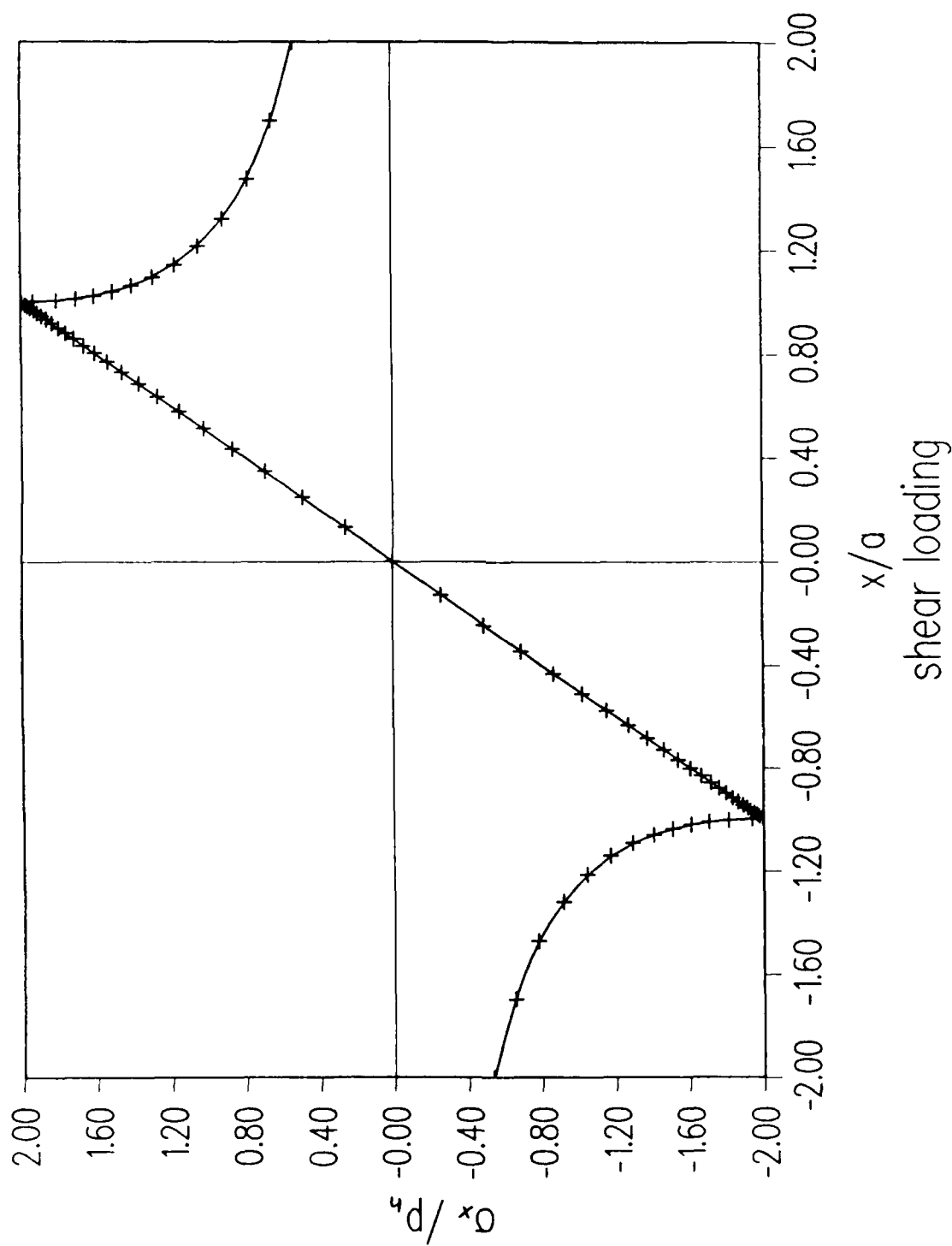


Figure 3-1. Finite element v/s Hertz solutions for stress  $\sigma_x$  under a shear loading.

# FEM SOLUTION VS. HERTZ CONTACT THEORY

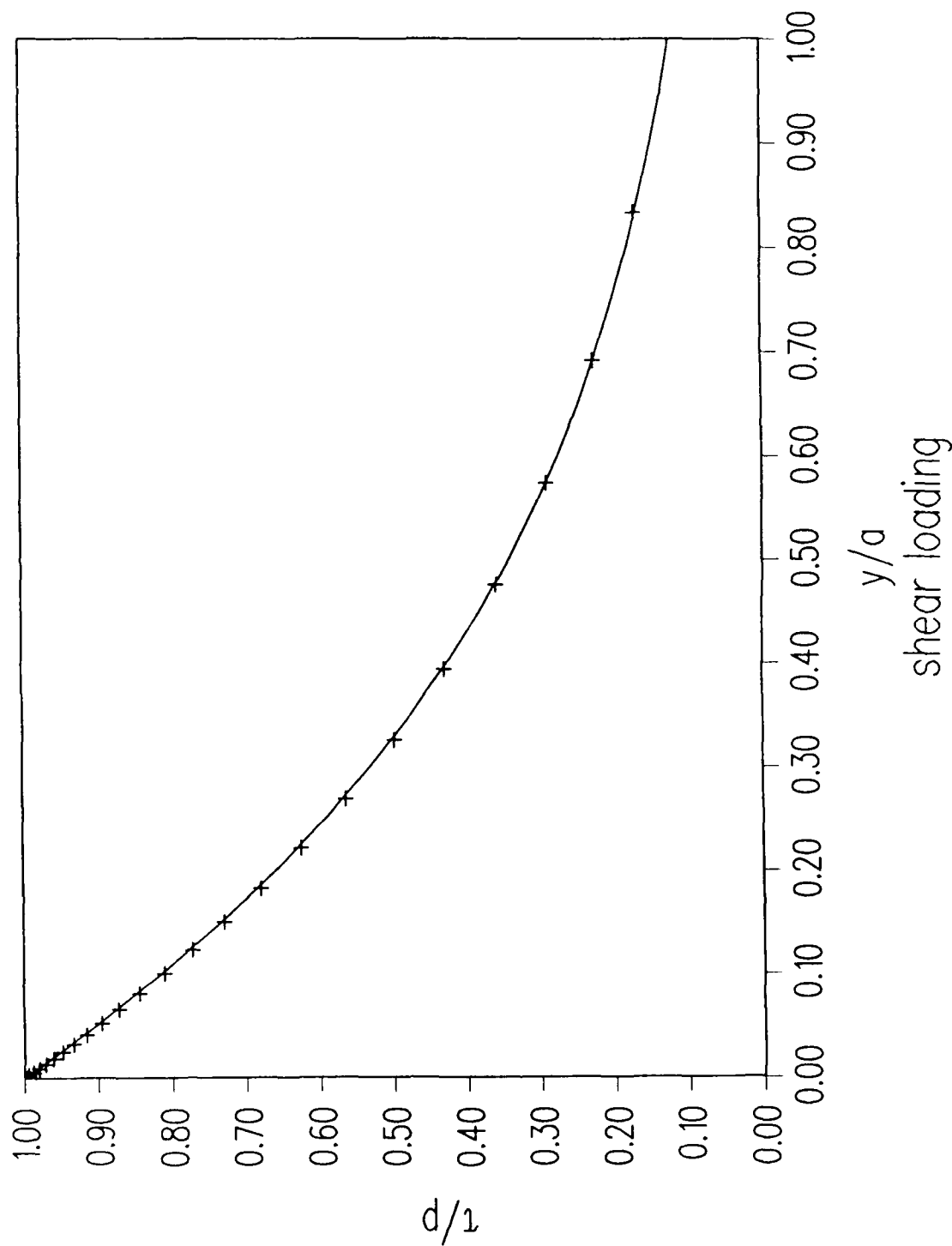


Figure 3-2. Comparison of the finite element and Hertz solution for sub-surface shear stress under a shear loading on the surface.

**Table 3-2**  
**Finite Element vs Fourier Solution**  
**Comparison of Normal Stresses**  
**at  $h/a = 0.25$**

$y/a$	Finite Element Solution		Fourier Solution	
	$\sigma_x/\sigma_h$	$\sigma_y/\sigma_h$	$\sigma_x/\sigma_h$	$\sigma_y/\sigma_h$
0.	1.412	1.00	1.421	0.9915
0.048682	1.232	0.9991	1.251	0.9921
0.11396	1.005	0.9918	1.026	0.9886
0.2500	0.5367	0.9628	0.5982	0.9617
0.55482	0.2453	0.8549	0.2547	0.8562
0.81478	0.1372	0.7540	0.1454	0.7552
1.000	0.08690	0.6737	0.09998	0.6877

**Table 3-3**  
**Finite Element vs Fourier Solution**  
**Comparison of Normal Stresses**  
**at  $h/a = 0.50$**

$y/a$	Finite Element Solution		Fourier Solution	
	$\sigma_x/\sigma_h$	$\sigma_y/\sigma_h$	$\sigma_x/\sigma_h$	$\sigma_y/\sigma_h$
0.	1.418	1.	1.428	0.9915
0.045625	1.267	0.9986	1.286	0.9917
0.10681	1.079	0.9909	1.099	0.9877
0.28369	0.6087	0.9432	0.6272	0.9436
0.50000	0.1906	0.8626	0.1470	0.8615
0.76010	0.1379	0.7595	0.1461	0.7608
1.00000	0.08410	0.6694	0.08928	0.6742



**Table 3-4**  
**Finite Element vs Fourier Solution**  
**Comparison of Shear Stress  $\tau_{xy} / \sigma_h$**

$y/a$	Finite Element Solution	Fourier Solution
0.	0.9962	0.9915
0.048682	0.8758	0.8790
0.11396	0.7248	0.7304
0.2500	0.4576	0.4587
0.55482	0.2463	0.2466
0.81478	0.1527	0.1515
1.000	0.1050	0.1110

**Table 3-5**  
**Finite Element vs Fourier Solution**  
**Comparison of Shear Stress  $\tau_{xy} / \sigma_h$**

$y/a$	Finite Element Solution	Fourier Solution
0.	0.9966	0.9915
0.045625	0.8931	0.8959
0.10681	0.7647	0.7700
0.28369	0.4695	0.4733
0.5000	0.2354	0.2350
0.76010	0.1413	0.1399
1.000	0.09053	0.09152

### 3.2 Parametric Studies

For the input properties outlined earlier in table 2-1, a number of finite element solutions are obtained for varying coating thicknesses. Note that the ratio of elastic modulus of the coating to that of the substrate is held fixed at 2.0 in all the finite element solutions. For practical applications, this represents a hard coat over a relatively soft substrate. An example would be ceramic type material over steel. The effect of coating thickness on various stress components under a normal elliptical loading is shown in figures 3-3 to 3-6. The high modulus coating tends to spread out the subsurface  $y$  force component over a broader area, thereby providing slightly lower values of  $\sigma_y$  as the coating thickness increases. Such a behavior is seen in figure 3-3. The presence of a coating results in an increase in  $\sigma_x$ , at the surface, as seen in figure 3-4. As the coating thickness reduces, the strains in the  $x$  direction in the coating tend to become equal to those in the substrate. This results in a higher value of  $\sigma_x$  in the coating due to its higher modulus. The discontinuity in stress at the coating/substrate interface, as seen in figure 3-4, corresponds to the jump in elastic modulus while a continuity in the strain component is maintained at the interface. Similar behavior is also seen in the variation of maximum shear stress, which is directly related to  $\sigma_x$  and  $\sigma_y$ . Figure 3-5 shows the location of the maximum shear stress for varying values of coating thickness. Note that for a thin coating, the maximum shear stress occurs very close to the surface. Figure 3-6 shows the variation of maximum shear stress on the surface. Again the higher value of shear stress with the presence of the coating results from the increased value of  $\sigma_x$ . Note that the maximum shear stress shown in figures 3-5 and 3-6, is really the principal shear resulting from  $\sigma_x$  and  $\sigma_y$  and it is not the orthogonal shear stress  $\tau_{xy}$ . In fact, by definition of the problem,  $\tau_{xy}$  is zero on the surface.

The influence of surface shear stress as a function of coating thickness is shown in figures 3-7 to 3-9. Figure 3-7 shows the variation in shear stress as a function of depth. As might be expected, the shear stress reduces with increasing depth. The surface shear stress acting in the negative  $x$  direction produces compressive  $\sigma_x$  before the center of contact and a tensile stress after the center of contact (figure 3-8). The peak value of these stresses increases as the coating thickness decreases to a limiting value equal to the product of stress with no coating present and the coating to modulus ratio. Similarly, high values of the maximum shear stress occurs near the edge of contact, and it tends to increase towards a limiting value as the coating thickness reduces, as seen in figure 3-9.

The surface temperature rise due to the applied thermal loading is shown in figure 3-10. The surface temperature climbs from the bulk temperature of the substrate at the start of the contact zone to a peak value near the trailing edge of contact where it falls off rapidly as the heat is conducted away through the solid. The presence of surface convection would cause the surface temperature to fall off more rapidly beyond the contact zone but would not significantly affect its value within the contact. Due to the thermal loading only, the variations of the  $x$  coordinate stress and the maximum shear stress are shown respectively in figures 3-11 and 3-12. The behavior of these stresses tends to follow the general pattern of the temperature distribution. The  $y$  coordinate stress,  $\sigma_y$ , and the orthogonal shear stress,  $\tau_{xy}$ , are both quite small.

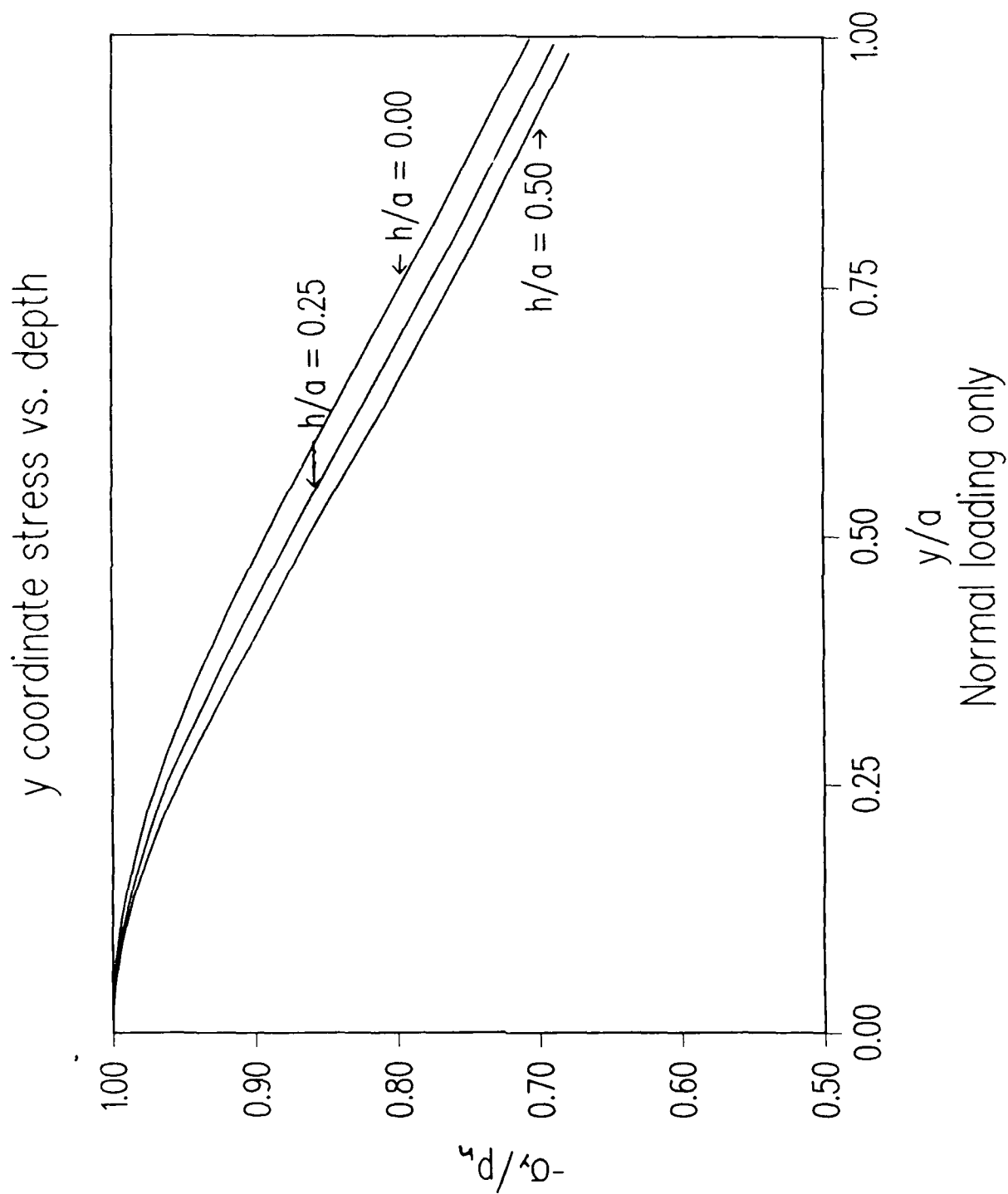


Figure 3-3. Coordinate stress,  $\sigma_y$ , as a function of depth under normal loading.

x coordinate stress vs depth

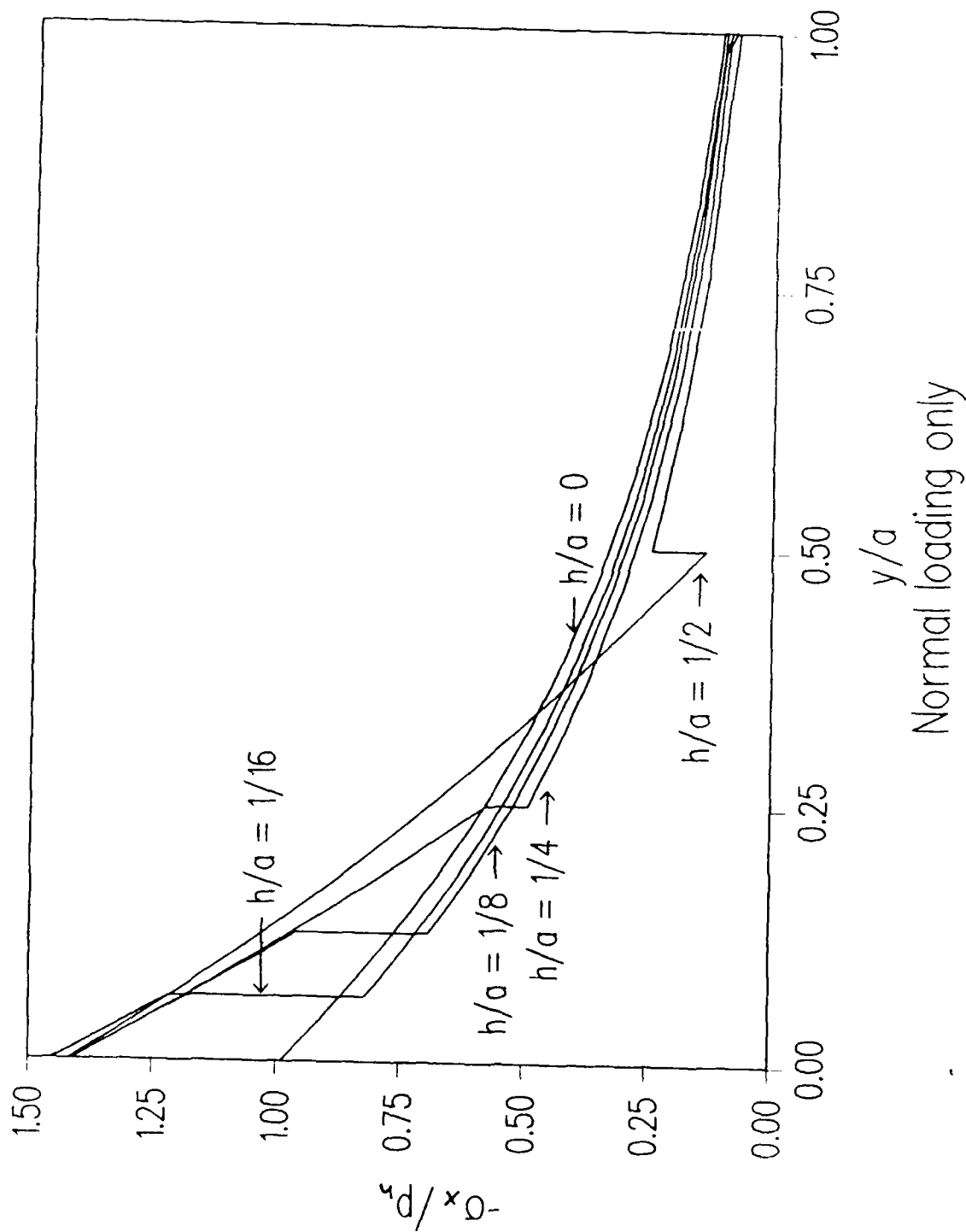


Figure 3-4. Coordinate stress,  $\sigma_x$ , as a function of depth under normal loading.

maximum shear stress vs. depth

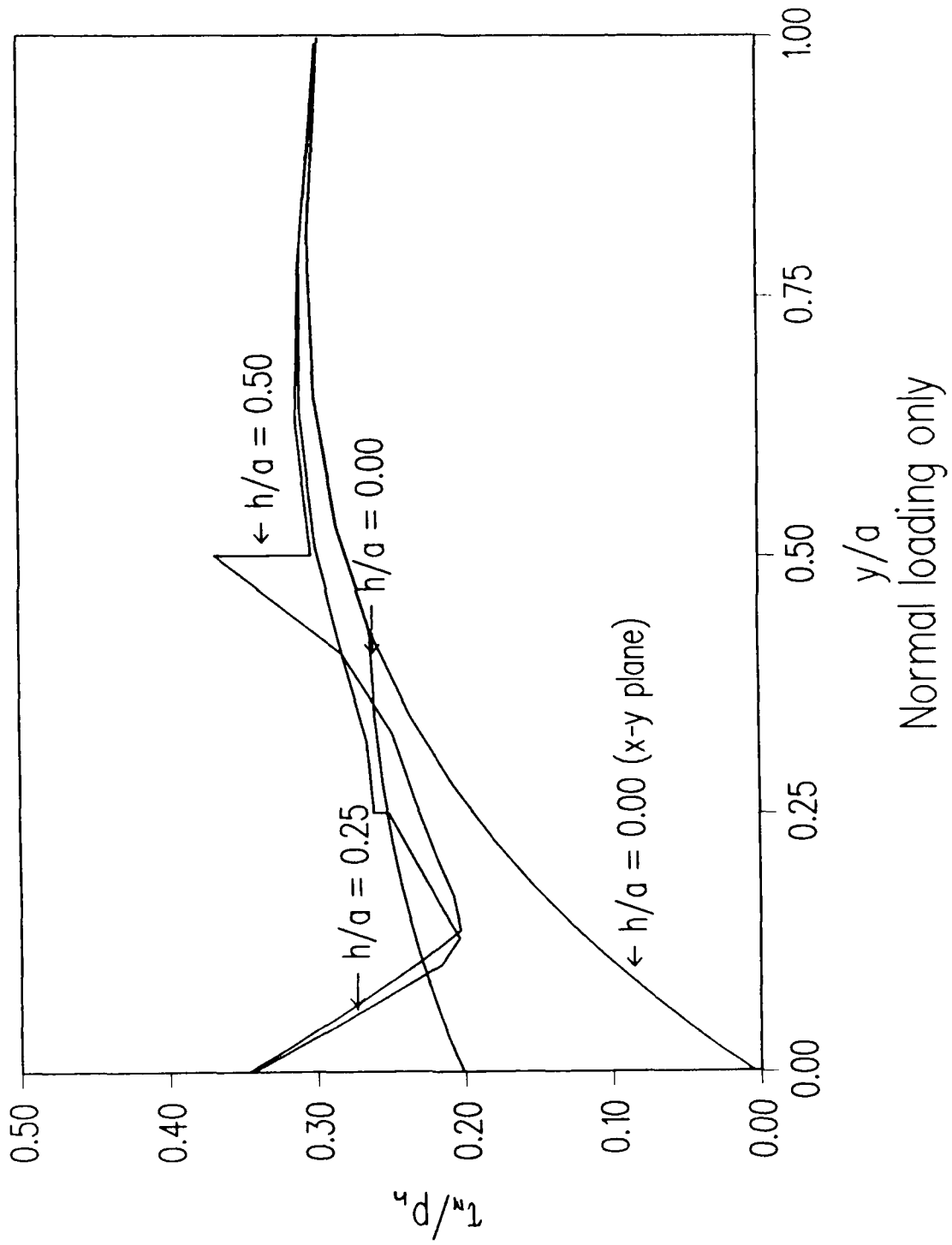
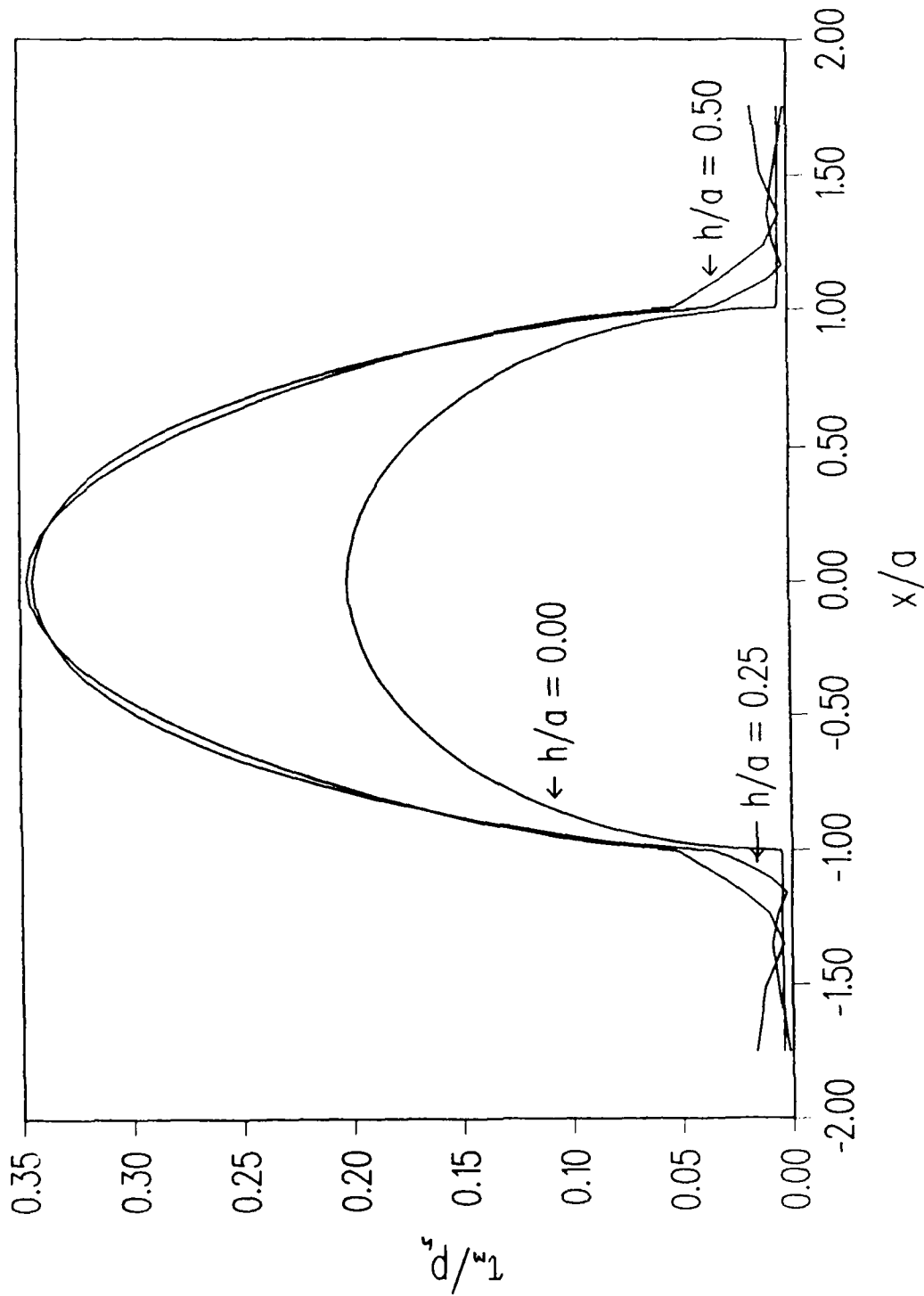


Figure 3-5. Maximum shear stress as a function of depth under normal loading.

maximum shear stress on surface



Normal loading only

Figure 3-6. Maximum shear stress at the surface under normal loading.

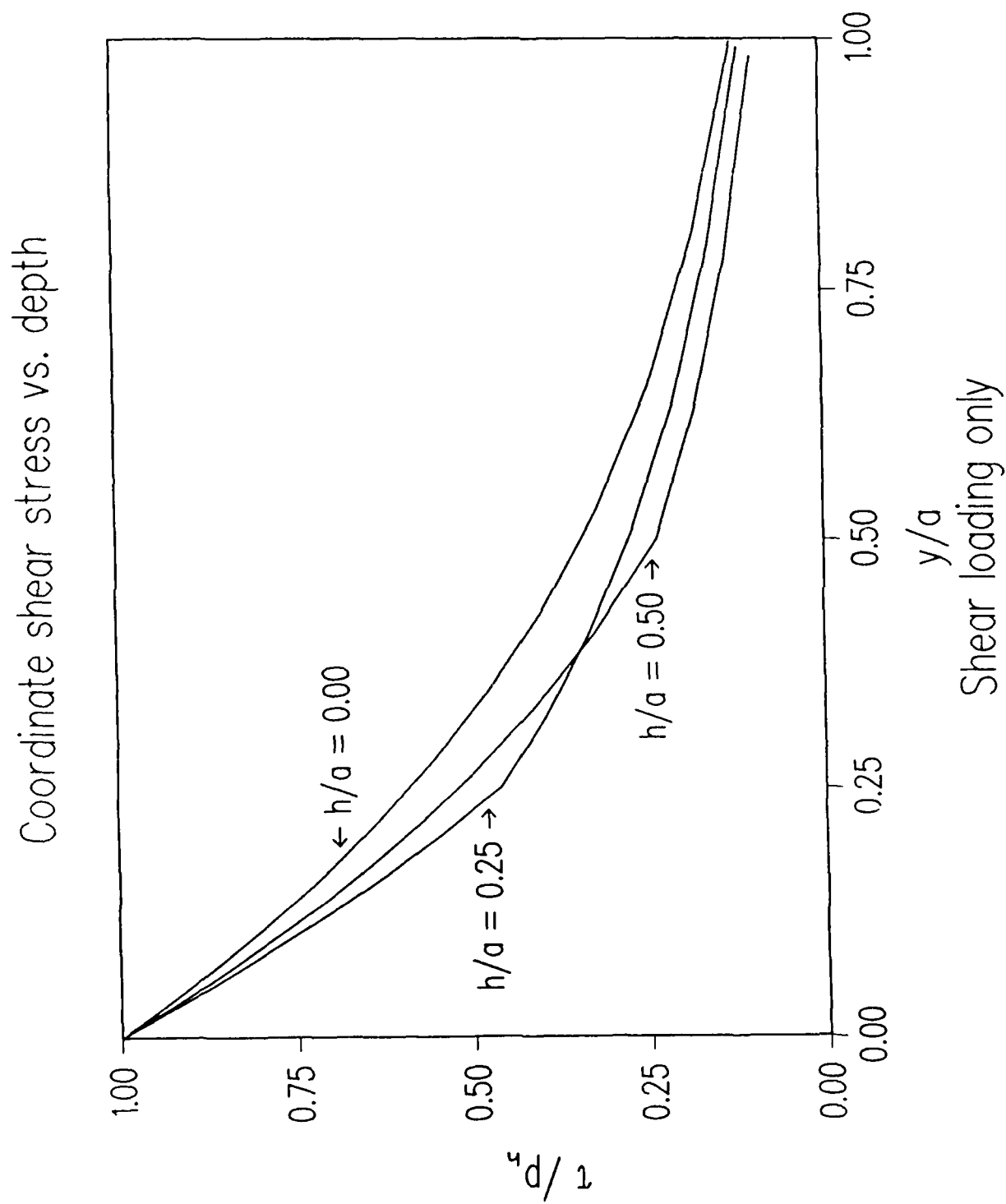


Figure 3-7. Coordinate shear stress,  $\tau_{xy}$ , as a function of depth under shear loading.

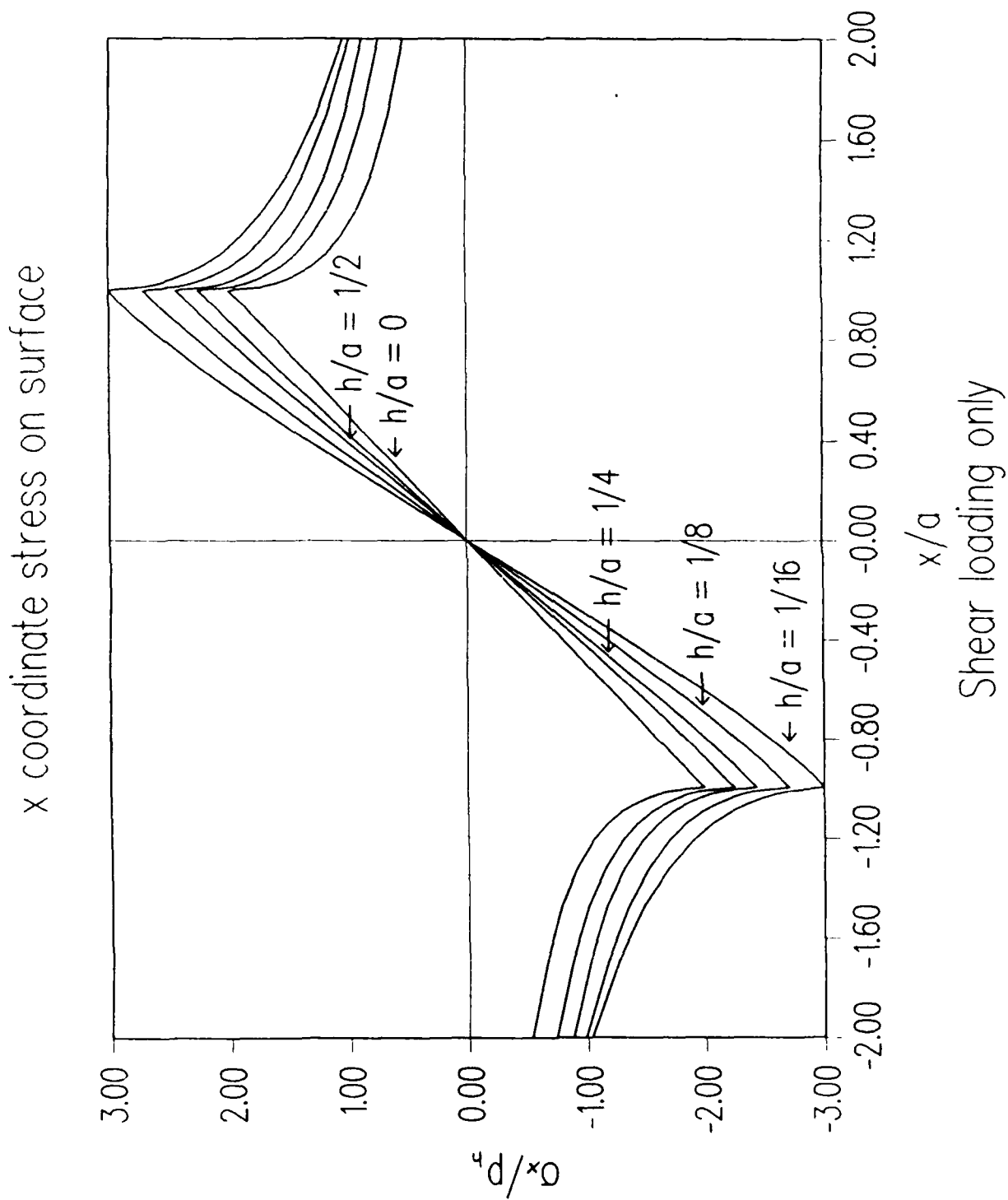


Figure 3-8. Coordinate stress,  $\sigma_x$ , on the surface under shear loading.



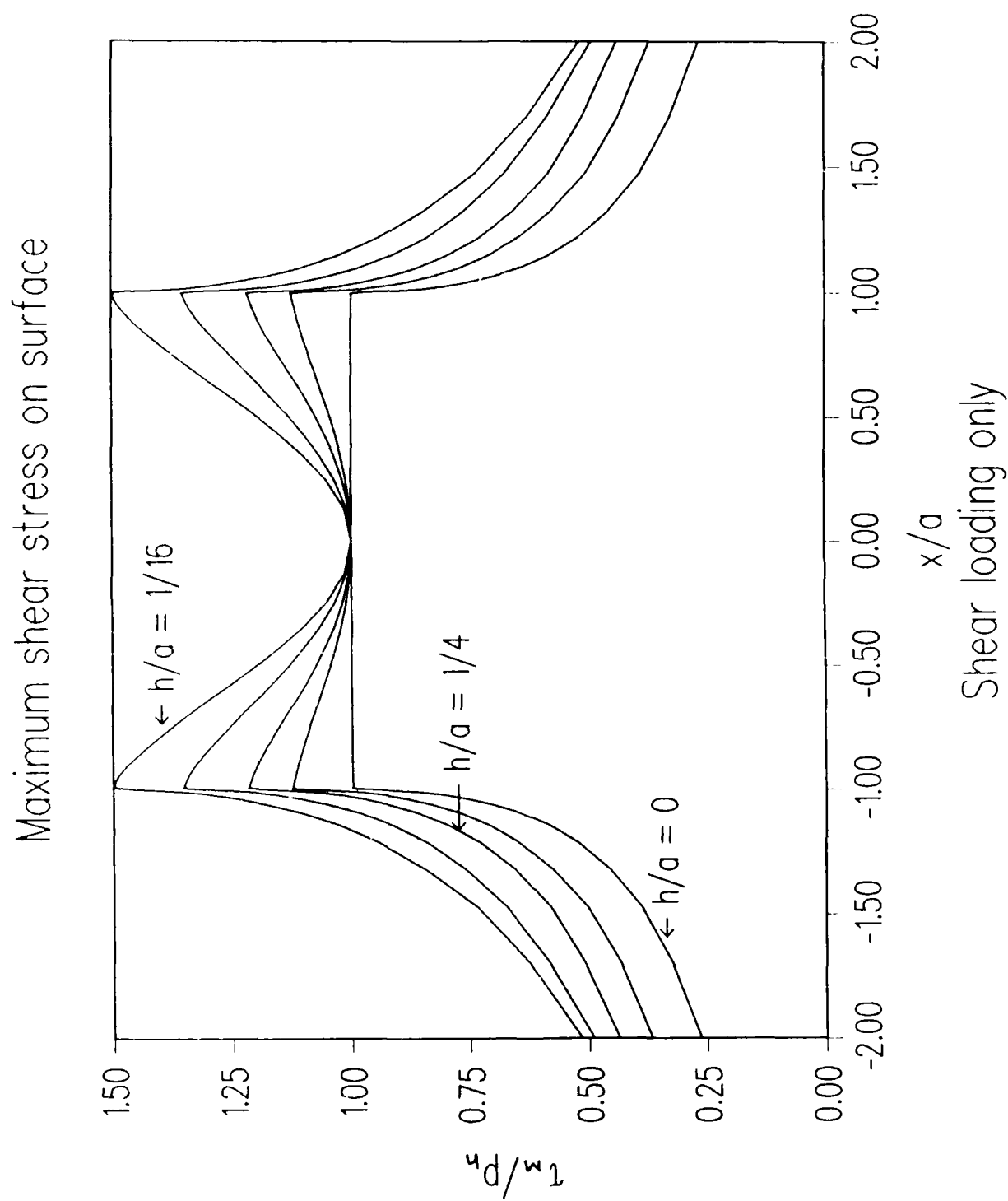


Figure 3-9. Maximum shear stress at the surface under shear loading.

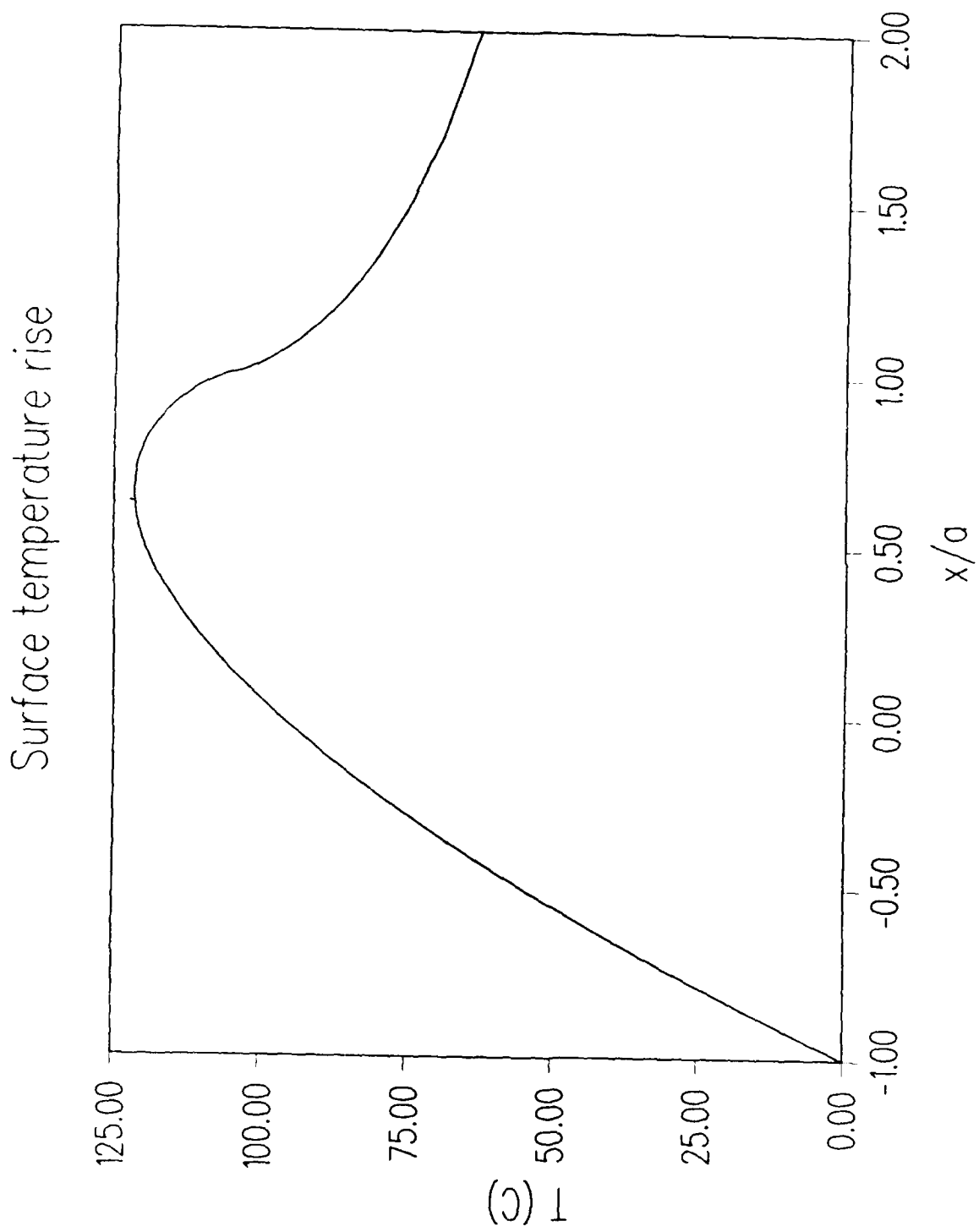


Figure 3-10. Surface temperature under the prescribed thermal loading.

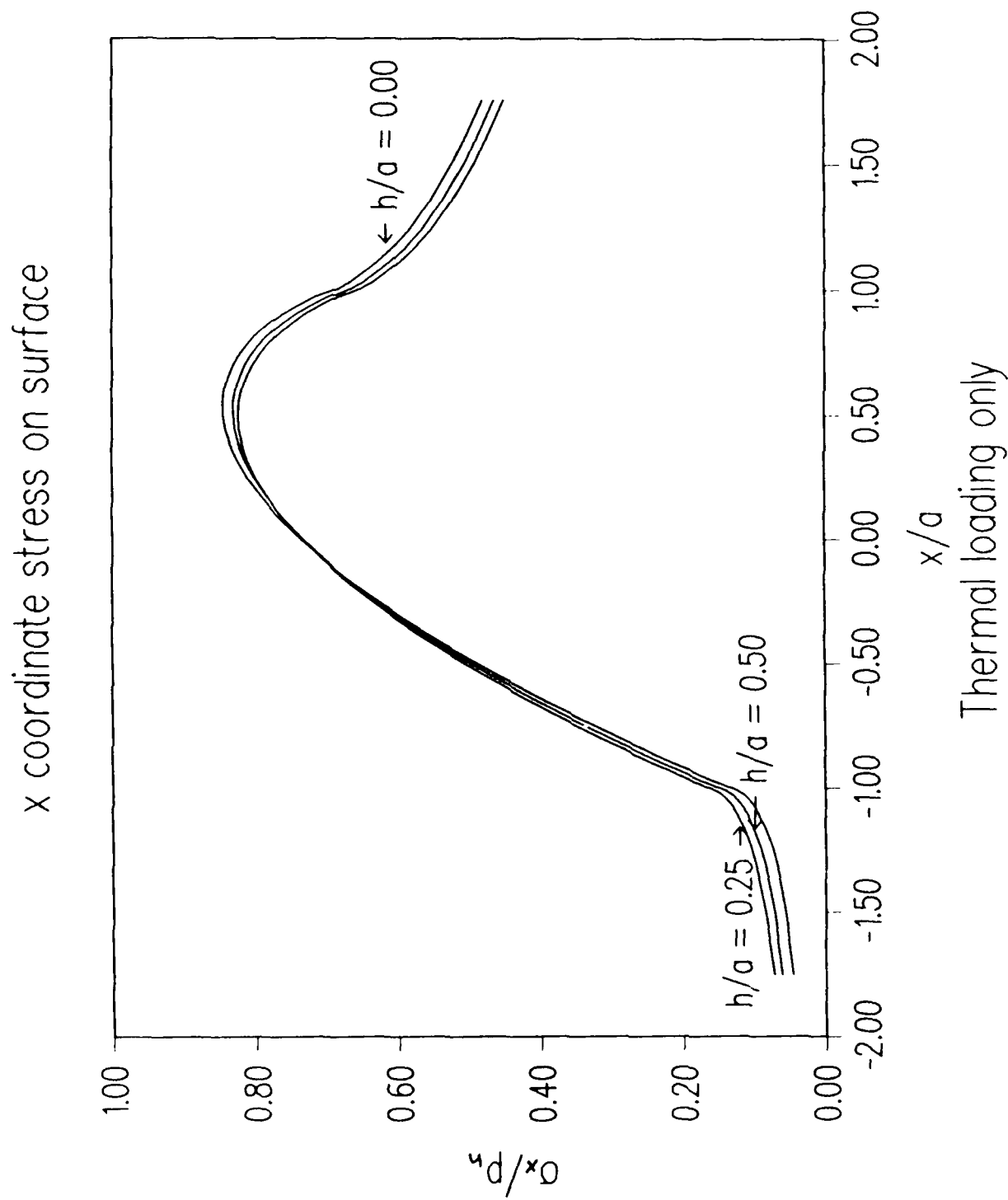


Figure 3-11. Coordinate stress,  $\sigma_x$ , on the surface under thermal loading.

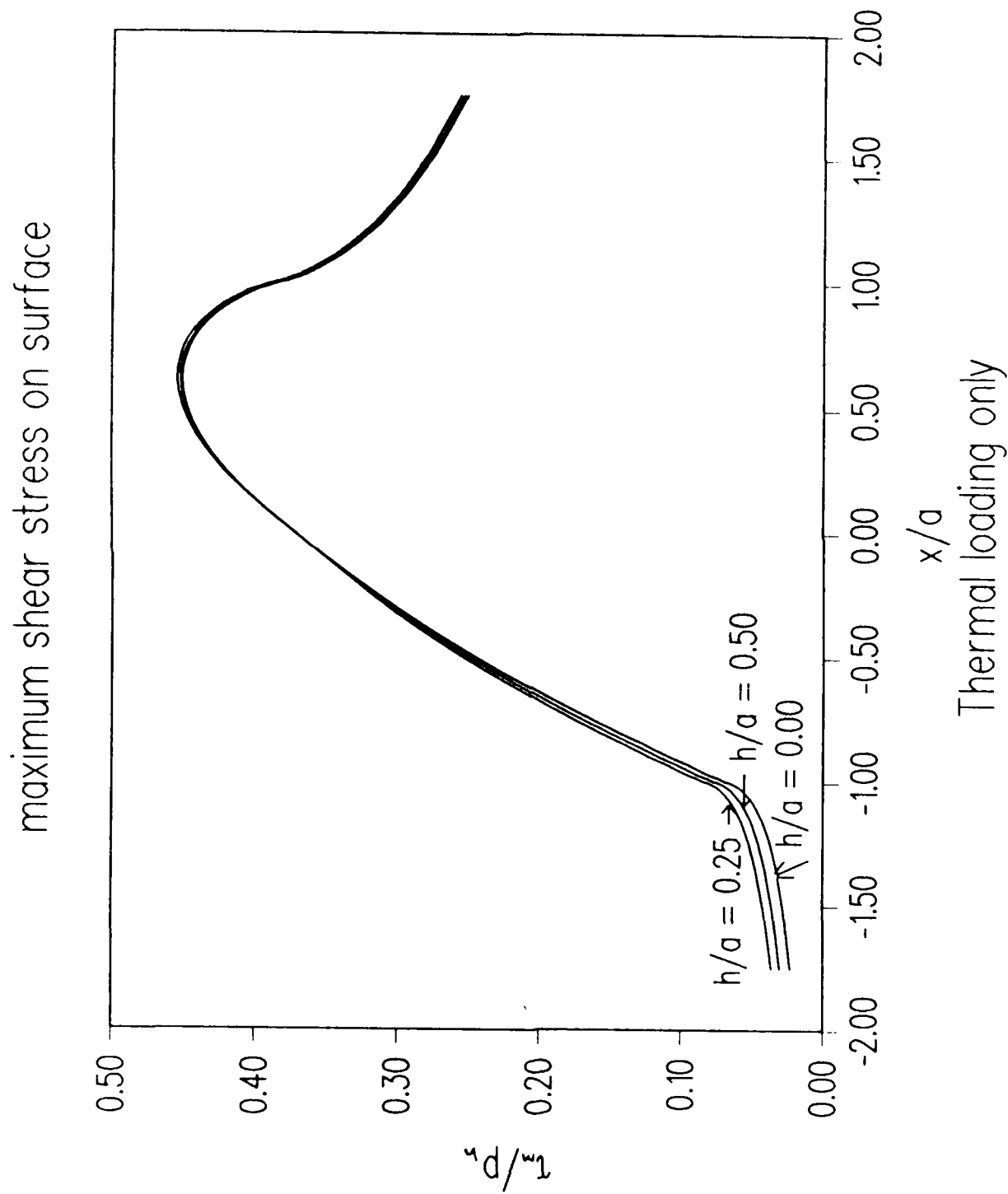


Figure 3-12. Maximum shear stress at the surface under thermal loading.

The finite element model provides detailed contour plots through the entire solid. Typical plots for the subsurface stresses and temperatures are shown in figures 3-13 to 3-21. The numerical values associated with each color shade are defined in the legend included with the contour map. Each color shade in the contour map represents a stress (or temperature) value that is less than or equal to the value defined in the legend. The aspect ratios in these plots have been distorted for clarity. The horizontal dimension of the plots spans four half widths along the surface. The three tic marks respectively correspond to the start, center and end of contact zone. The vertical dimension covers only one half width. Figures 3-13 and 3-14 show respectively the normal and shear stress profiles for the Hertzian case. Note the maximum shear stress occurs at a certain depth (figure 3-14). This depth is generally used in computation of fatigue life in rolling bearings where the material is subjected to cyclic loading. For a relatively thin coating,  $h/a = 1/8$  the coordinate stress,  $\sigma_x$  and the maximum shear stress  $\tau_m$  are shown in figures 3-15 and 3-16 respectively. Note the discontinuity in stresses at the coating/substrate interface. The coordinate shear stress  $\tau_{xy}$ , however, is, continuous across the interface, as seen in figure 3-17.

The temperature contours used in the thermal stress computations are shown in figure 3-18. Note the thermal boundary layer behavior that occurs in a high-speed contact. For the purpose of comparison, a second case of thermal loading is obtained by reducing both the Peclet Number (which represents a reduction in speed) and the thermal conductivity of the coating by a factor of 2. The resulting temperature contours, as shown in figure 3-19, indicate both an increased depth of propagation into the solid (due to reduced Peclet Number) and high values of the surface temperature (due to decreased thermal conductivity). The solutions for the coordinate stress,  $\sigma_x$ , corresponding to these two temperature distributions are shown in figures 3-20 and 3-21.

The above results clearly demonstrate the technical feasibility of the finite element approach. Since all stresses are scaled relative to the maximum applied pressure or shear stress, the solutions may be applied to any applied loading. Similarly, all linear dimensions are scaled relative to the contact half width, thus the results may be applied to a wide range of coating thicknesses. However, results are shown for only one value of the ratio of the elastic modulus of the coating to that of the substrate. Also, for the purpose of proving the technical feasibility of the modeling approach, a simple two-dimensional line contact configuration is considered above. This permits validation of the finite element solutions with those obtained by other numerical techniques. In general, however, the finite element modeling approach is applicable to any contact geometry. For effective practical application of the model, dimensionless solutions similar to the ones discussed above may be generated over a large range of geometrical and operational parameters to establish a design data base. This data base can then be readily used to carry out design optimization for any given application.

To further establish the design significance of modeling approach, a series of results, similar to the ones discussed above, are obtained by executing the computer program LAYER, based on the Fourier transform approach. The results are applied to a 30 mm bore solid-lubricated ball bearing, operating at 70,000 rpm with a thrust load of 1,000 N and a rotating radial load of 500 N. The bearing dynamics analysis based on the computer program ADORE [14] reveals that for such an application typical values of contact stresses and half width assume

$$\frac{\sigma_x}{p_h} \times 10^5$$



Figure 3-13. Stress contours for  $\sigma_x$  under normal loading without a coating.



Figure 3-14. Contours of maximum shear stress under normal loading without a coating.

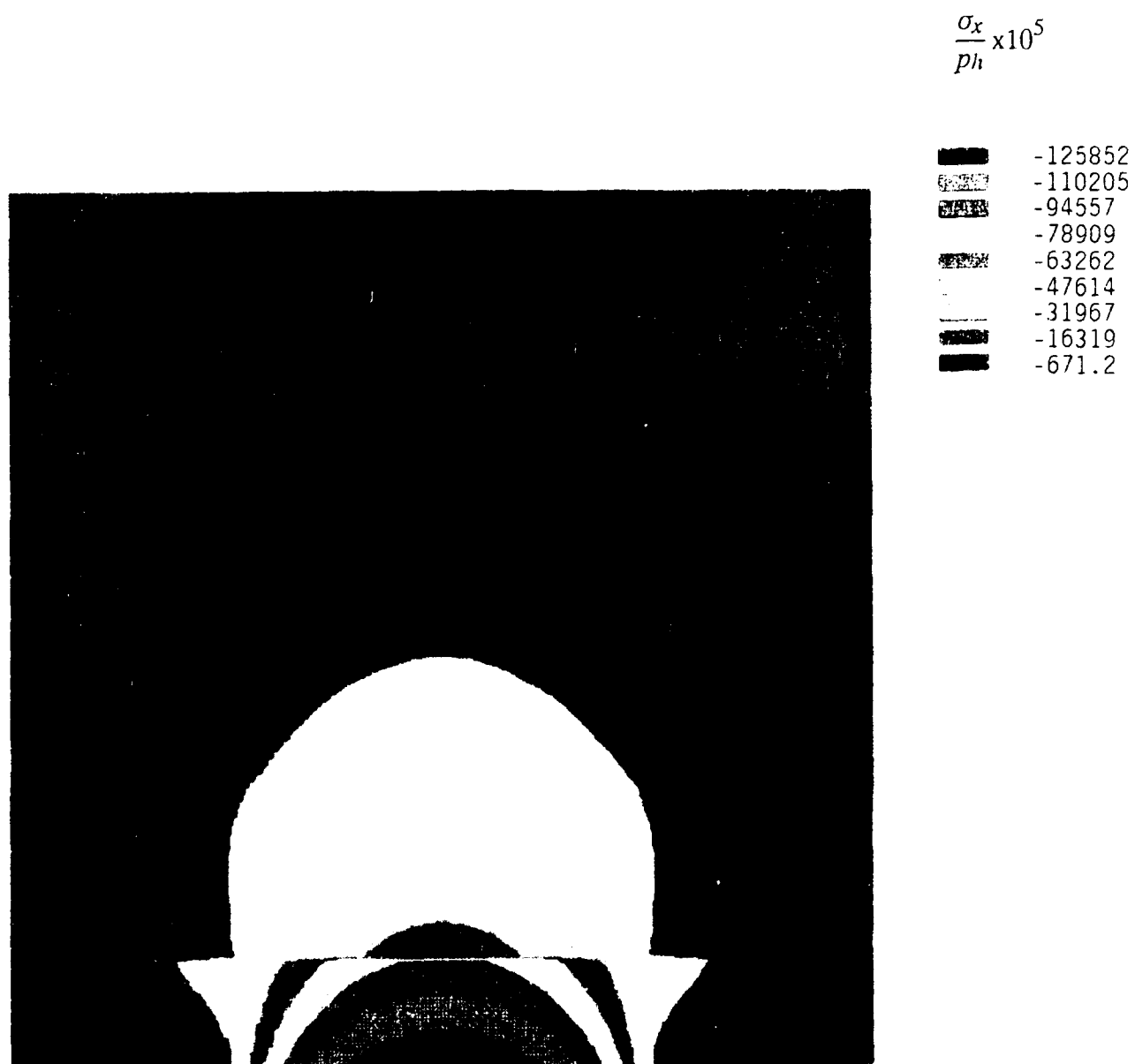


Figure 3-15. Contours of stress,  $\sigma_x$ , under normal loading with  $h/a = 1/8$ .



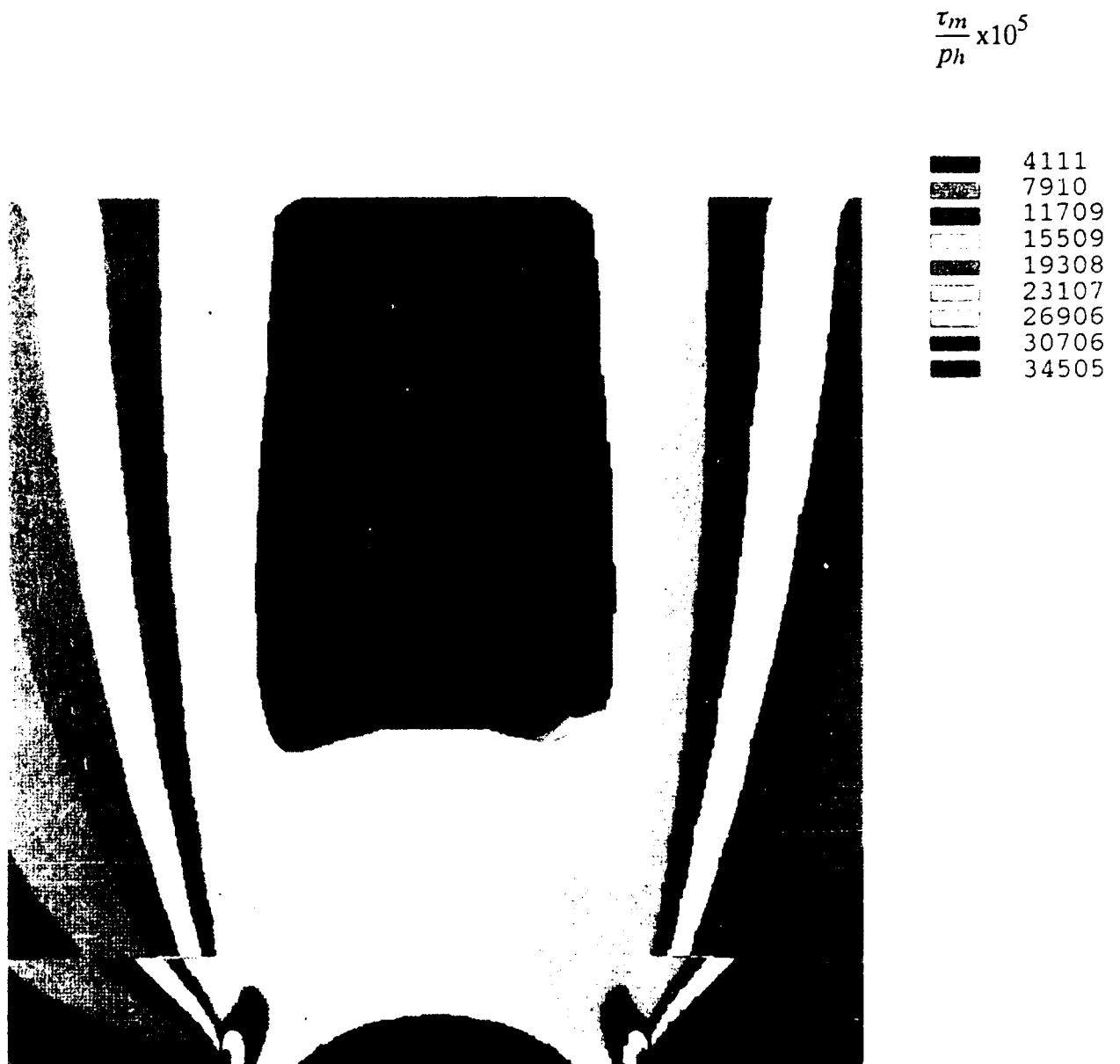


Figure 3-16 Contours of maximum shear stress under normal loading with  $h/a = 1/8$ .

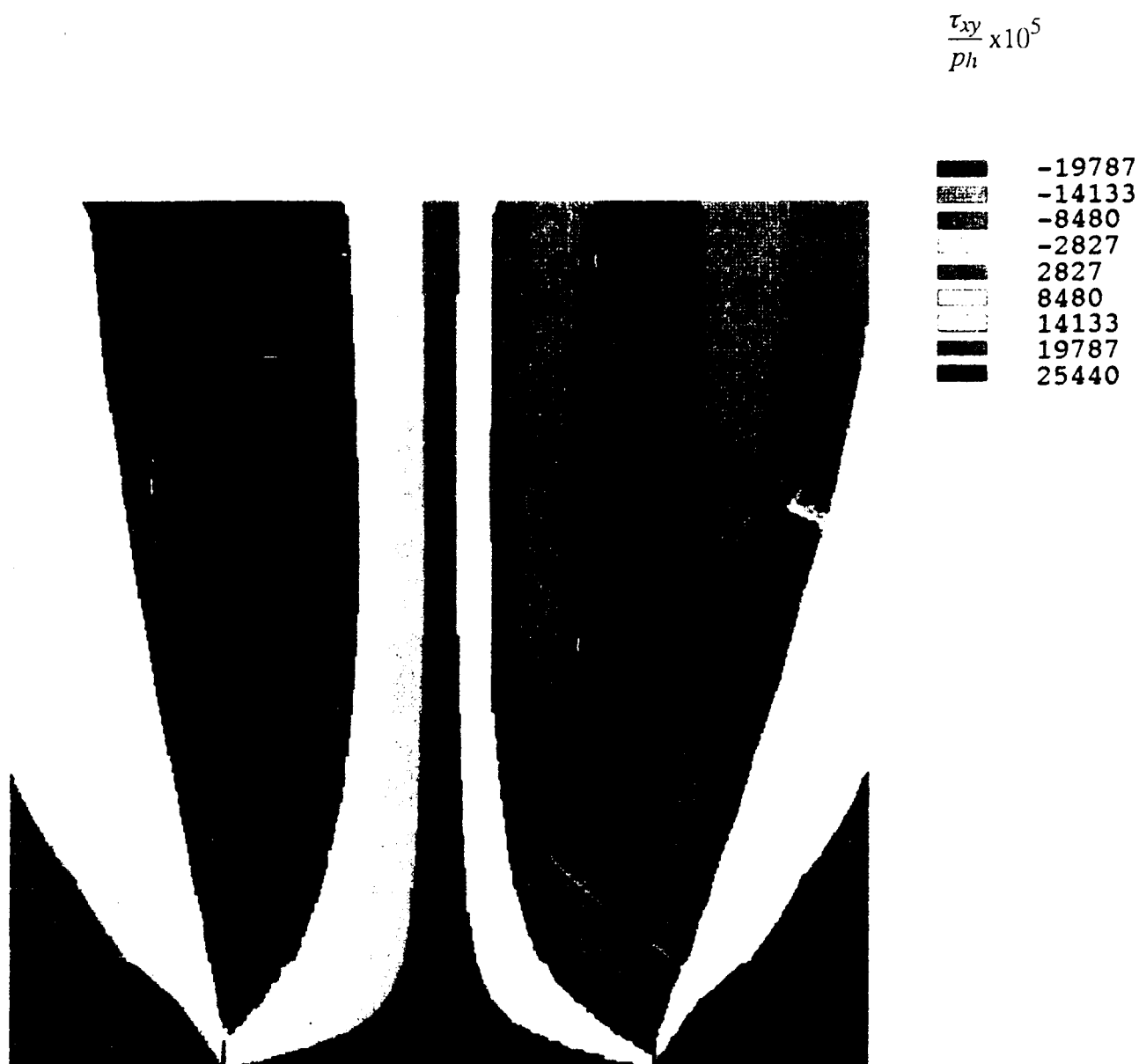


Figure 3-17. Contours of coordinate shear stress,  $\tau_{xy}$ , under normal loading with  $h/a = 1/8$ .

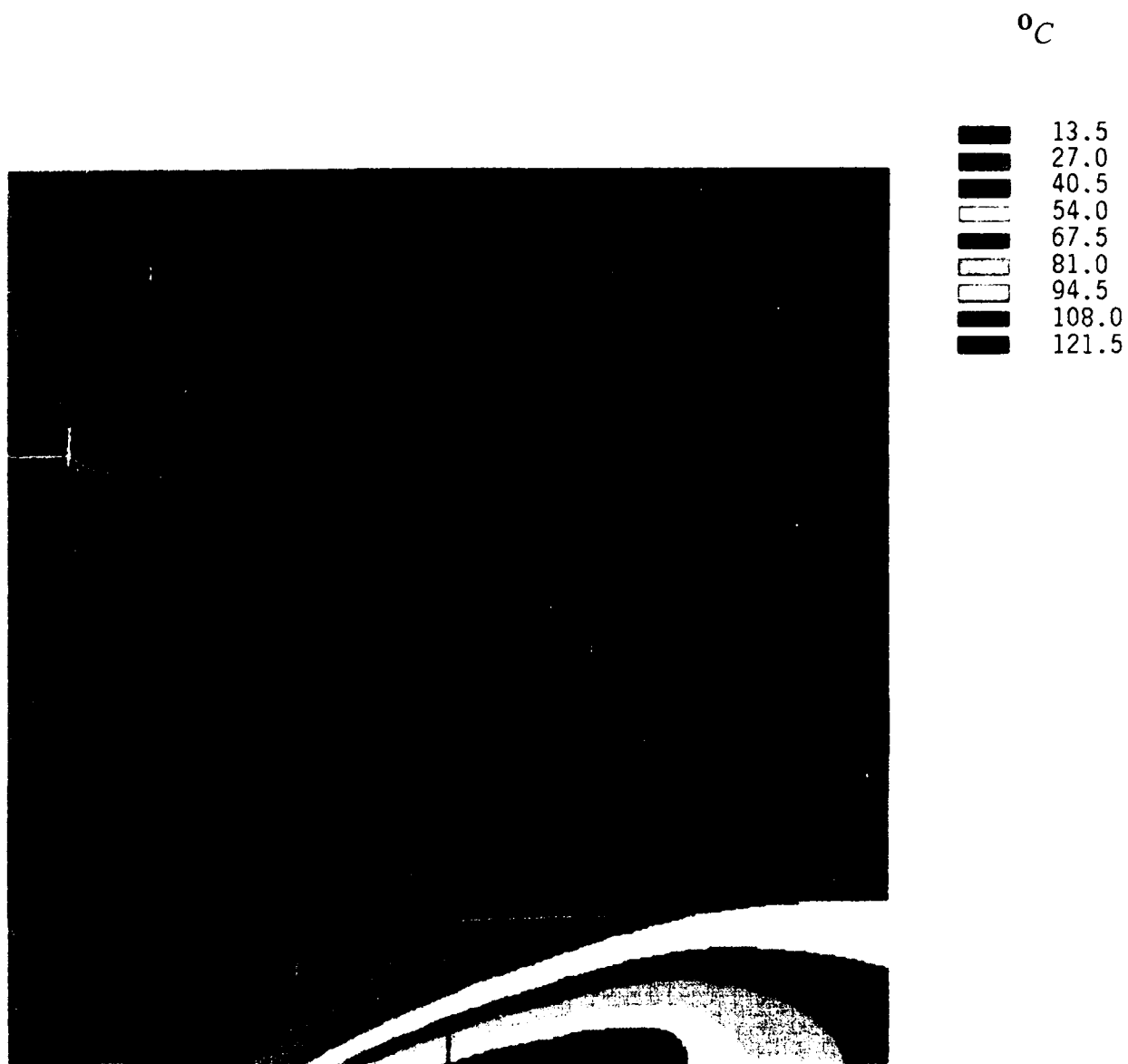


Figure 3-18. Temperature map used in the thermal stress computations.

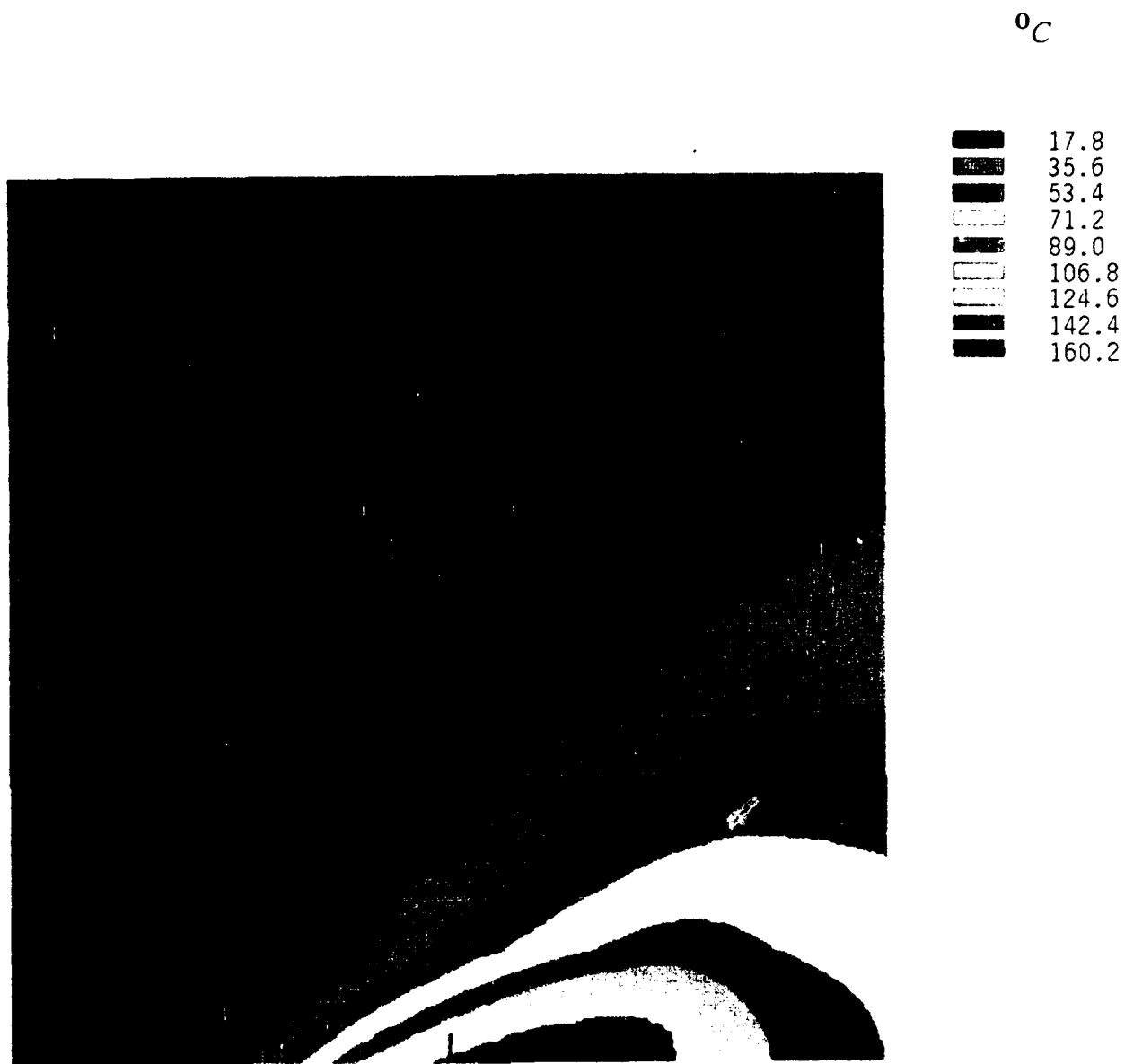


Figure 3-19. Temperature map under reduced Peclet number and increased thermal conductivity of the coating.

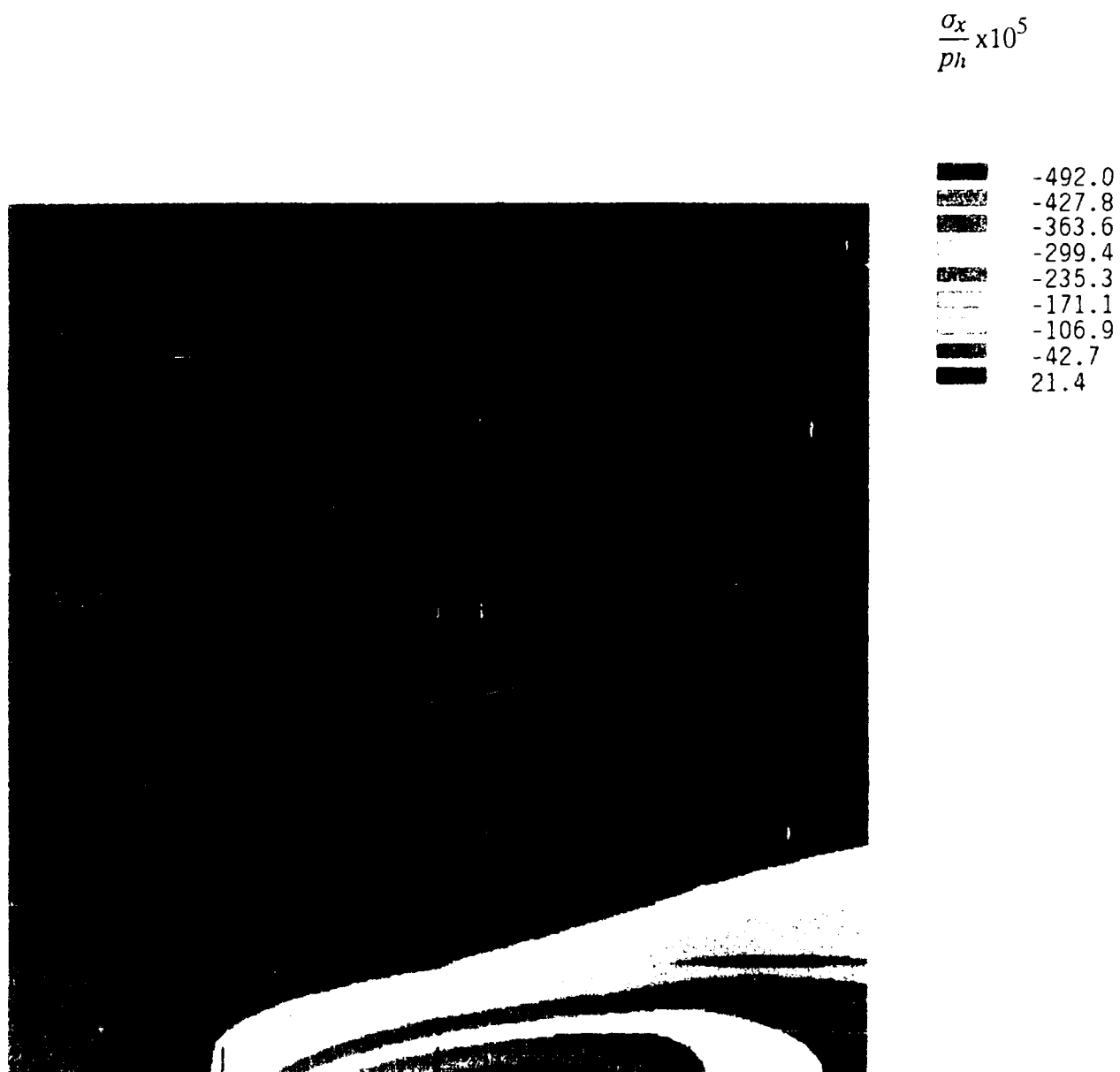


Figure 3-20. Contours of  $\sigma_x$  under the temperature field of figure 3-18.

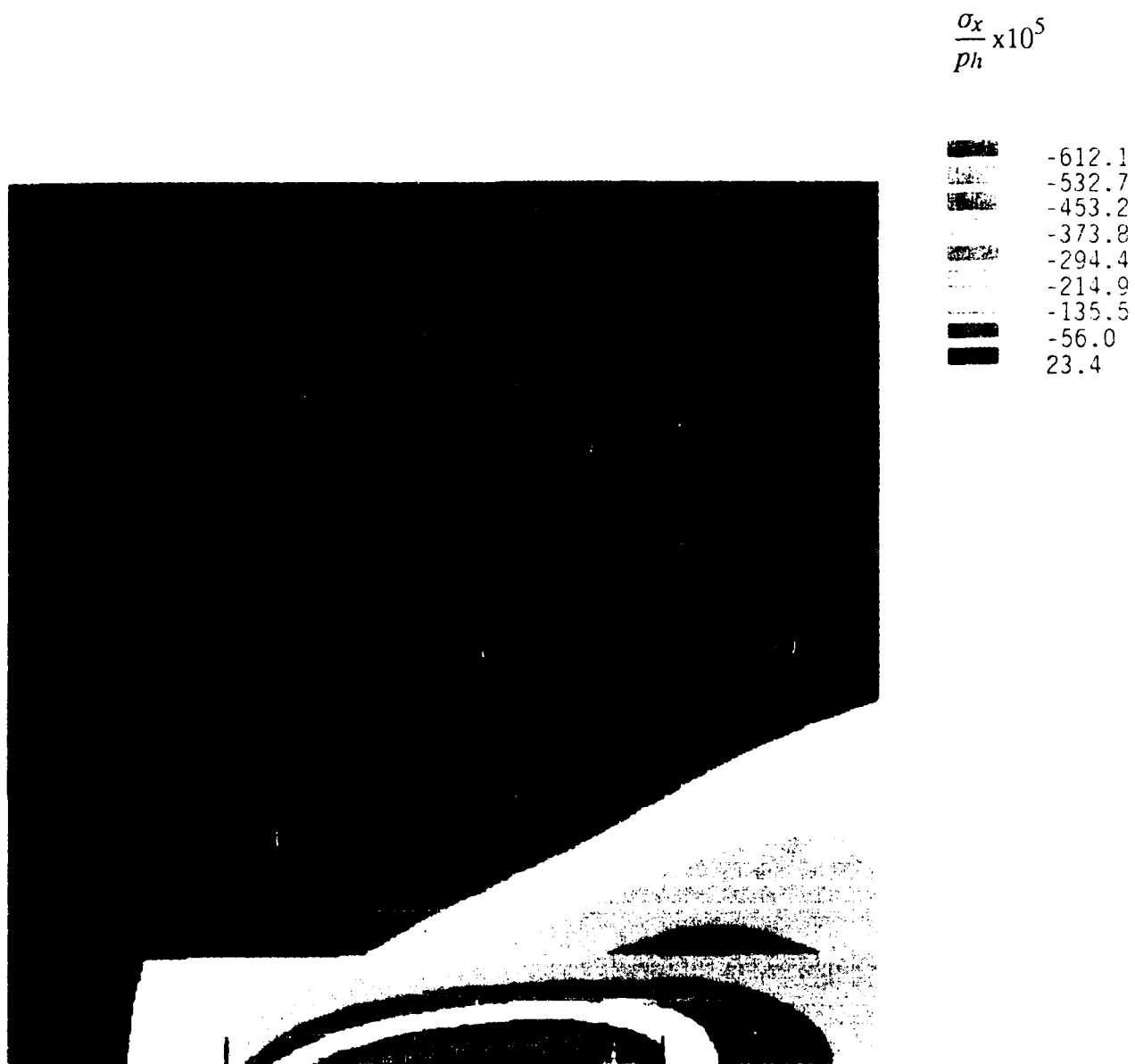


Figure 3-21. Contours of  $\sigma_x$  under the temperature field shown in figure 3-19 for reduced Peclet number.

values of  $10^9$  Pa and  $10^{-5}$  M. When the dimensionless results obtained by executing the program LAYER are applied to this problem, pertinent stresses may be related to the applied coating thickness and therefore, practical guidance on the coating substrate design may be obtained. Typical results are shown in figure 3-22, where the maximum coordinate shear stress, which occurs close to the edge of the contact, is plotted as a function of coating thickness for two different values of the elastic modulus of the coating. The coating surface is loaded with an elliptically distributed normal loading with a maximum pressure of  $10^9$  Pa. The substrate is assumed to be a bearing steel with a modulus of  $2.0 \times 10^{11}$  Pa. The higher coating modulus is representative of ceramic materials, while the lower modulus value simulates a relatively soft coating of some solid lubricant materials. The results show that the interfacial shear stresses first increase with increasing coating thickness, and beyond a certain value of the coating thickness, the shear stress begins to drop. Thus some guidance on required "break-away" shear stress may be obtained. This may help determine the coating application techniques and procedures.

In addition to the normal loading discussed above, the coating surface may be subjected to a shear stress result from relative sliding due to ball slip or skid. In order to simulate such a condition, additional solutions are obtained with an elliptically distributed shear stress. The peak value of the shear stress is assumed to be  $10^8$  Pa, which corresponds to a friction coefficient of 0.10. As already discussed earlier with the finite element solutions, the shear stress at the surface induced tension at the coating/substrate interface. Again, the maximum tension occurs near the entrance to the contact zone. Typical results are shown in figure 3-23. Tension at the interface tends to reduce with increasing coating thickness for both the hard and soft coats.

The solutions of figures 3-22 and 3-23 may be superimposed to obtain a combined effect of normal and shear loadings on the coating surface. Thus failure under both tension and interfacial shear may be modeled, and substantial guidance for the required break-away stresses may be obtained.

Aside from the mechanical loading discussed above, the thermal loading, resulting from the heat generated at the coating surface, becomes important particularly when the thermal coefficient of expansion of the coating is greatly different from that of the substrate. For example, the coefficient of thermal expansion for ceramic material, such as SiN, is  $2.9 \times 10^{-6}$  M/M/°C, while that of M50 bearing steel is  $12.3 \times 10^{-6}$  M/M/°C. Under such a thermal mismatch, the interfacial shear stresses may be greatly altered, and it is essential to revise the coating/substrate adhesion or break-away stress requirements. Under the simplified assumptions of the temperature field, discussed earlier in section 2, figure 3-24 shows an increase in the maximum orthogonal shear stress at the coating/substrate interface with the increasing temperature rise in the contact for two different values of coating thickness. Once again, these stresses may be linearly superimposed on those obtained with mechanical loading to derive the required failure limits for the combined effects.

The above discussion illustrates application of the model results to an actual problem.

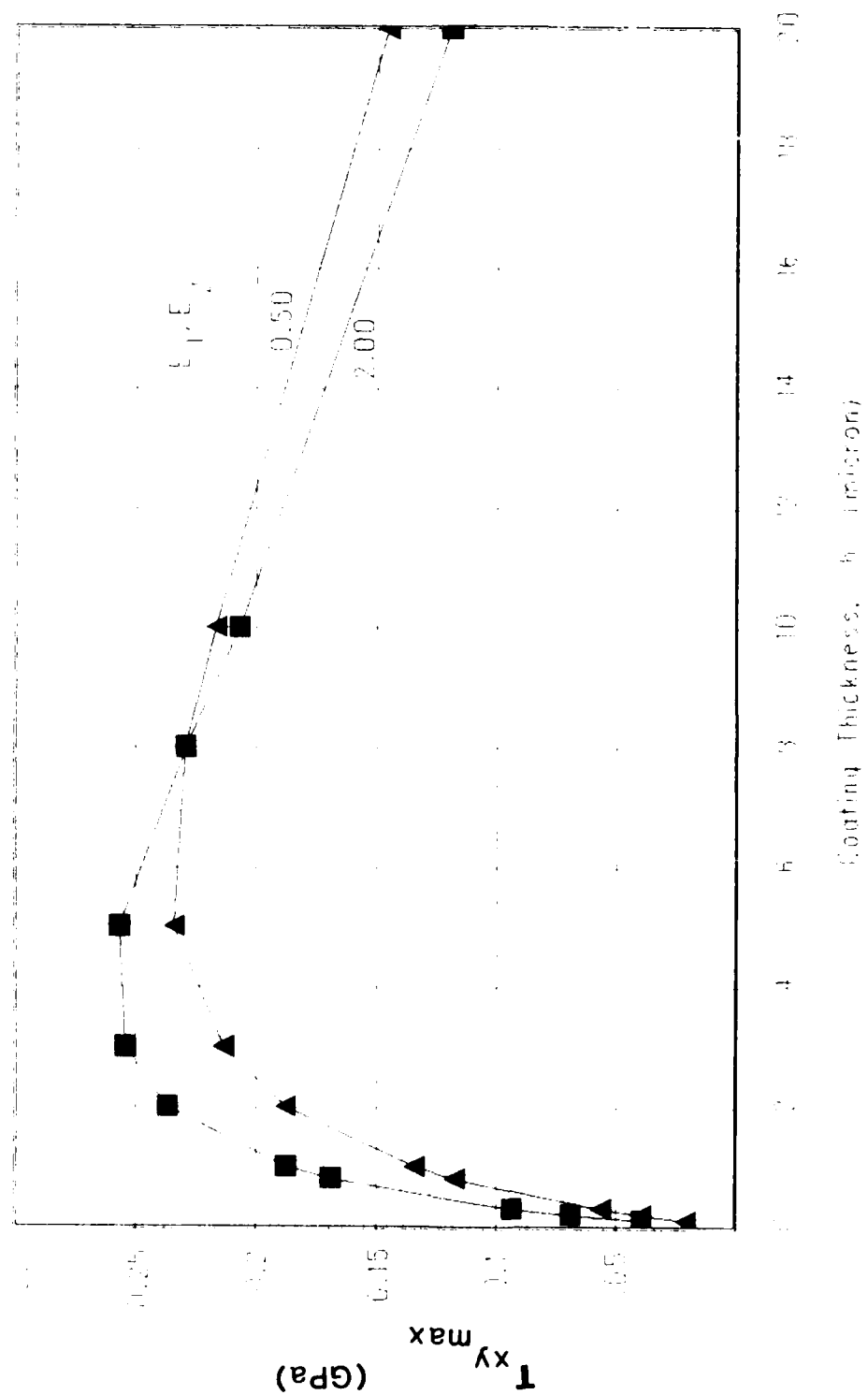


Figure 3-22. Maximum coordinate shear stress,  $\tau_{xy}$ , as a function of coating thickness under a maximum contact pressure of  $1.0 \times 10^9$  Pa.



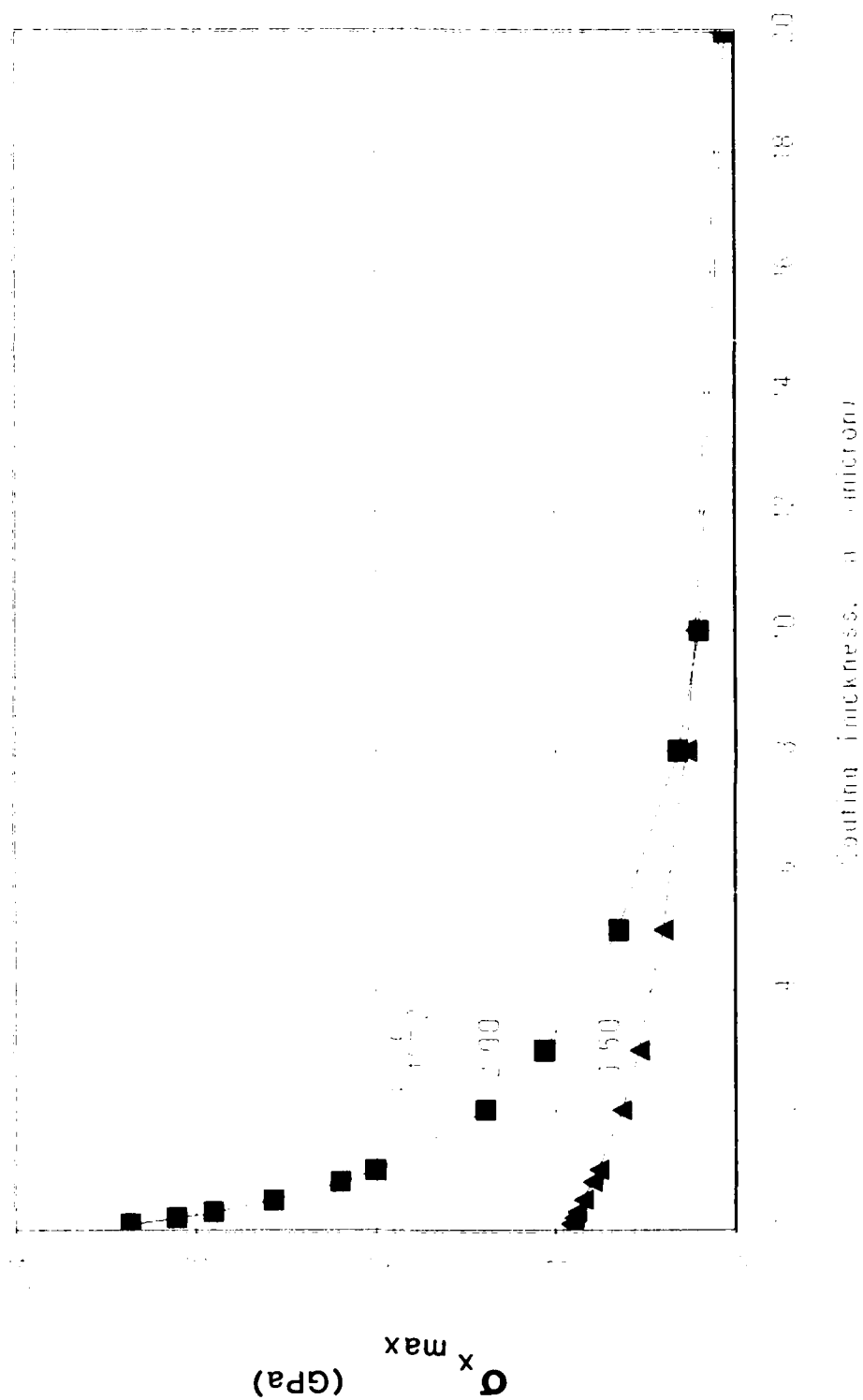


Figure 3-23. Maximum coordinate shear stress,  $\sigma_x$ , under an elliptical surface shear with peak amplitude of  $1.0 \times 10^8$  Pa.

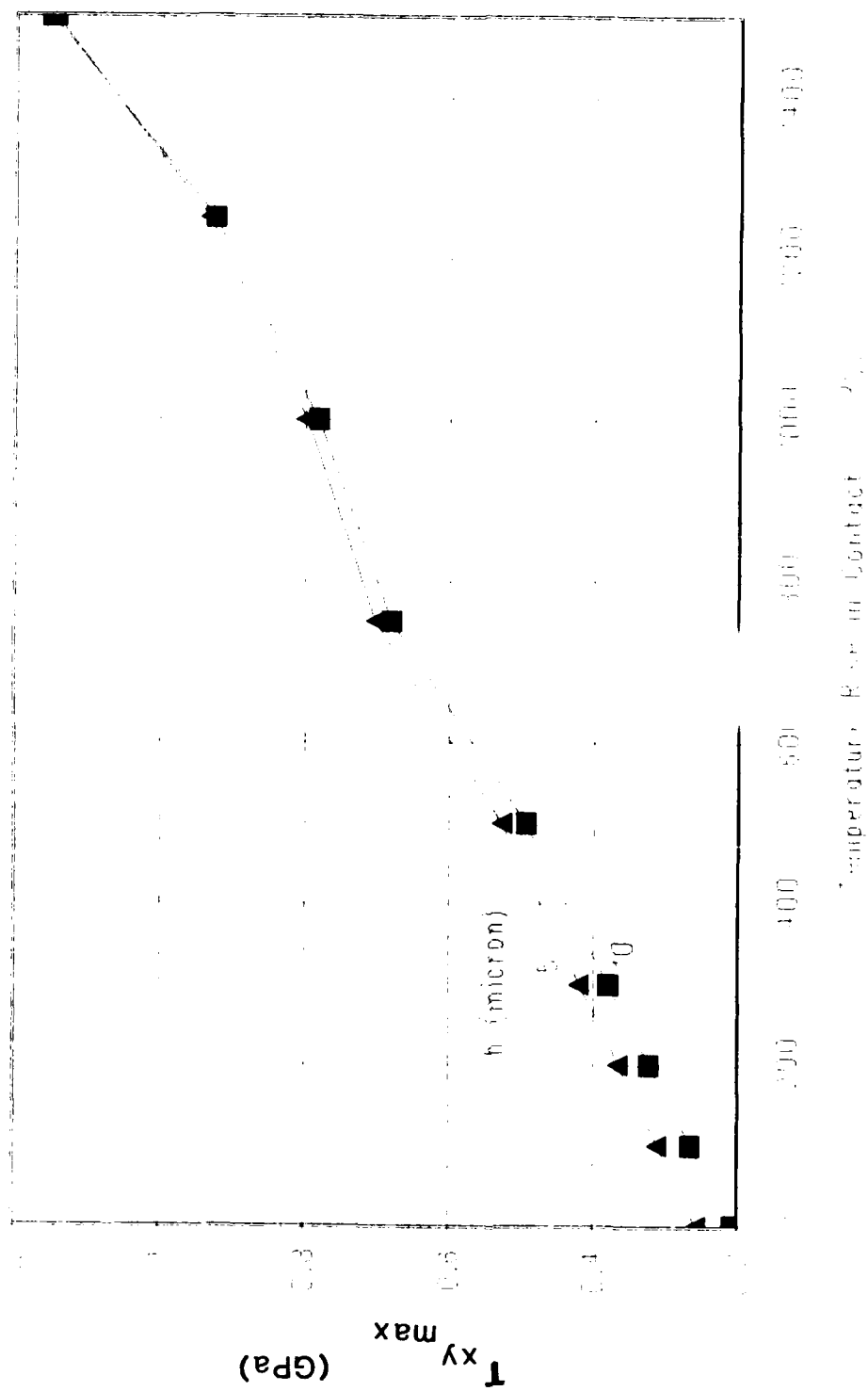


Figure 3-24. Maximum coordinate shear stress,  $\tau_{xy}$ , as a function of temperature rise at the coating/substrate interface.

Once again, it may be emphasized that for most design applications, it may not be necessary to solve the integral problem, once a design data base of dimensionless solutions over a range covering the design parameters is available. In fact, after proving the technical feasibility of the modeling approach in the present Phase I, the generation of such a design data base shall be undertaken in Phase II of this project. In addition to the two-dimensional problem, discussed above, the Phase II work scope shall include modeling of the more complicated three-dimensional problem. The following discussion of a preliminary three-dimensional model provides added support for the finite element approach to modeling any contact geometry.

### 3.3 Three-Dimensional Finite Element Modeling

Modeling of a three-dimensional contact greatly increases both the mass storage and computing speed requirements, which adds to the limitations of PC-ANSYS and the use of personal computer systems for finite element modeling. However, for the purpose of feasibility demonstration, once again, PC-ANSYS is used to model a simple three-dimensional problem. The grid structure is kept relatively coarse, in order to make the finite element code workable within the storage limitations of the available personal computer system. A uniform pressure over a rectangular contact region is assumed on the coating surface. The element geometry and loading conditions are schematically shown in figure 3-25. The aspect ratio is somewhat distorted but the complete grid is shown. The shaded area represents the load region. The surface boundaries are defined by  $x = \pm 5a$  and  $z = 5b$  with  $b/a = 2$ . The depth of the solid corresponds to  $y = 5a$ . A symmetry condition in  $z$  direction is imposed by requiring zero normal deflection at  $z=0$ . As in the two-dimensional model, discussed above, a zero deflection condition is imposed at the  $y$  boundary of the solid, and remaining surfaces, with the exception of the contact zone, are assumed to be free of any loads. The PC-ANSYS supplied three-dimensional isoparametric element having 8 nodes and 3 degrees of freedom at each node is used. All material properties are assumed to be identical to those used in the two-dimensional modeling.

Solutions are first obtained without any coating. A consistency check on the solutions is obtained by computing the surface loads and comparing them with the applied boundary conditions. Figure 3-26 shows the results. The discrepancy in the finite element solutions is clear when the plotted solution is compared with a rectangle. Considering the rather coarse grid used in generating this solution, this deviation is quite acceptable. Typical stress solutions are shown in figure 3-27, where the variation in  $\sigma_x$  with depth is plotted at various values of  $z/a$  in the  $y-z$  plane, defined by  $x=0$ .

Similar to the above solutions, figures 3-28 and 3-29 show solutions with a coating of thickness,  $h = 0.25a$ . The variation of computed stress  $\sigma_x$  along the  $x$  axis is shown in figure 3-28 while the distribution along the  $z$  direction is plotted in figure 3-29. For comparison, the solutions for the no coating case ( $h/a = 0$ ) are also plotted. Again, the deviations from a true rectangle are quite acceptable in view of the coarse grid. A contour map of the surface loading, as shown in figure 3-30, further elaborates on the computed surface loading.

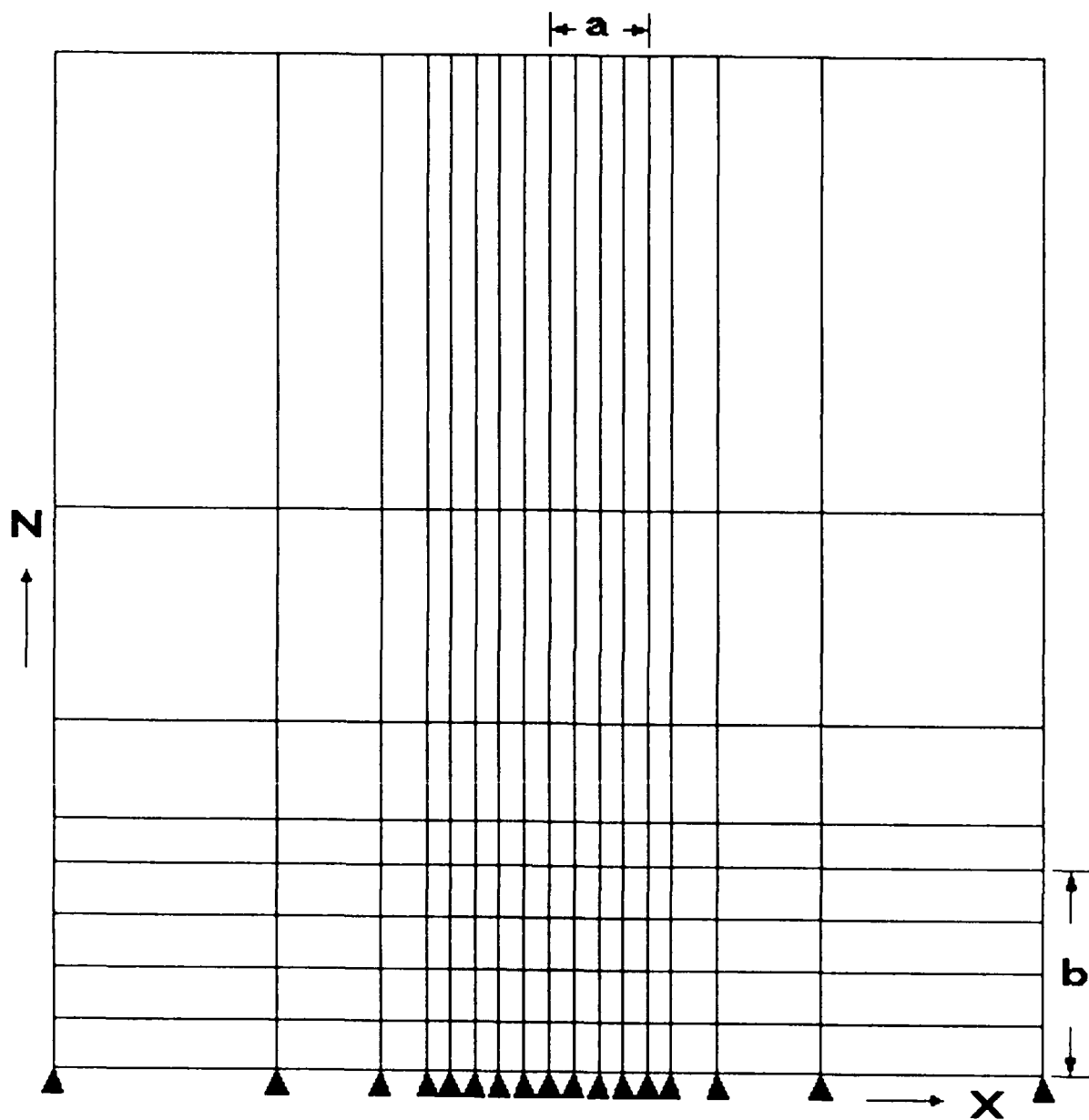


Figure 3-25. Finite element grid structure on the surface for a three-dimensional model.

# Y COORDINATE STRESS FOR 3-D MODEL

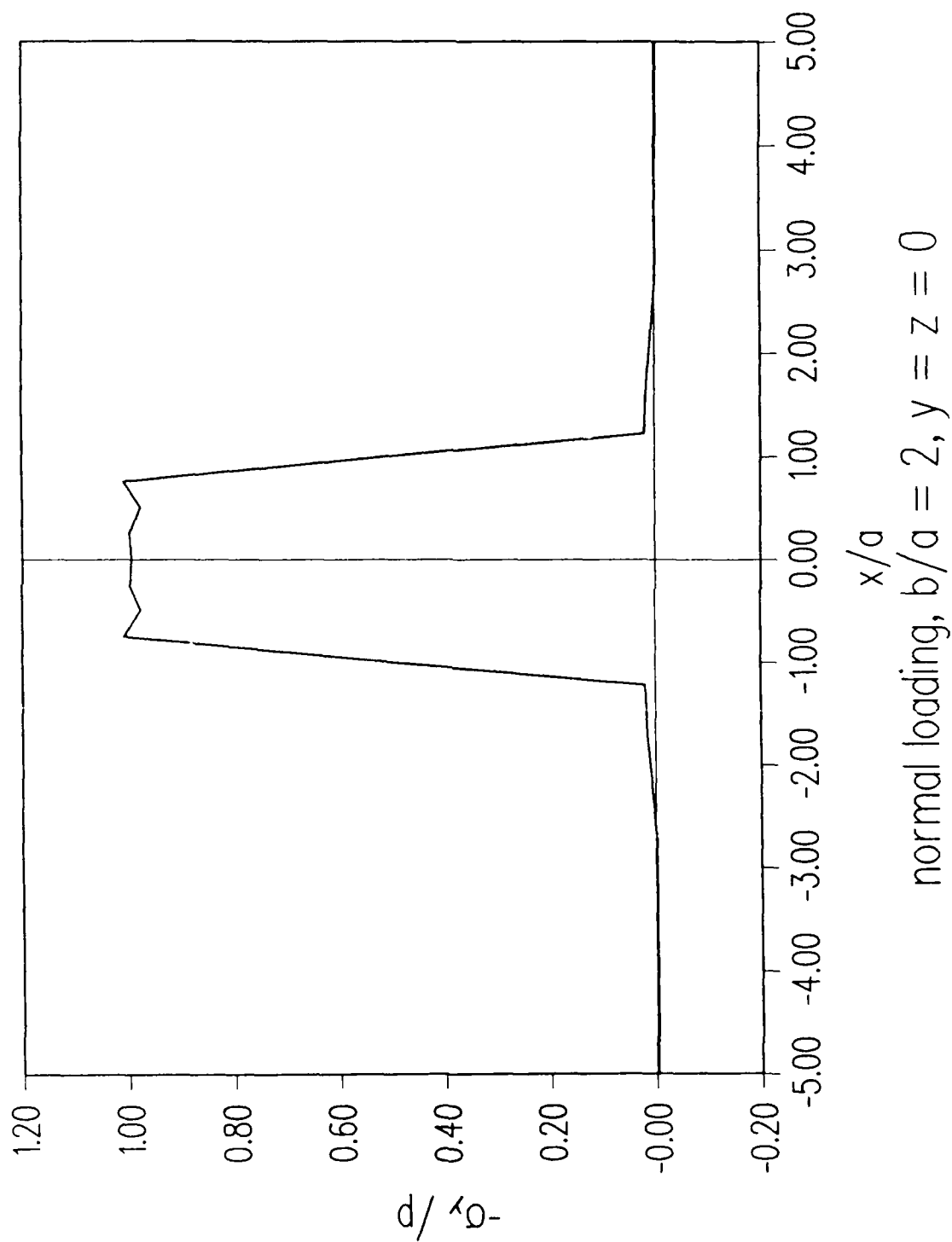


Figure 3-26. Surface stress,  $\sigma_y$ , as computed by the finite element model under the rectangular load.

# X COORDINATE STRESS FOR 3-D MODEL

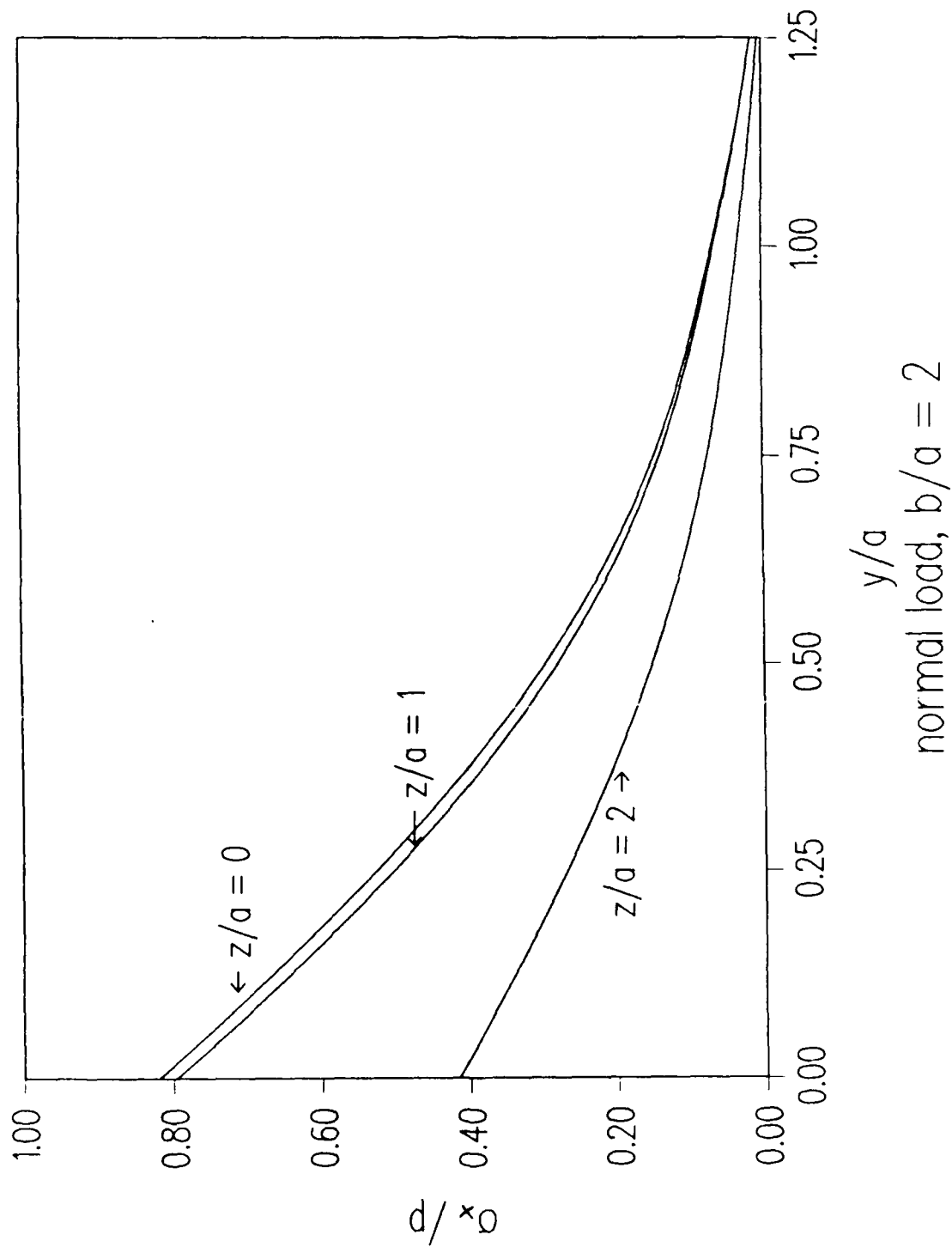
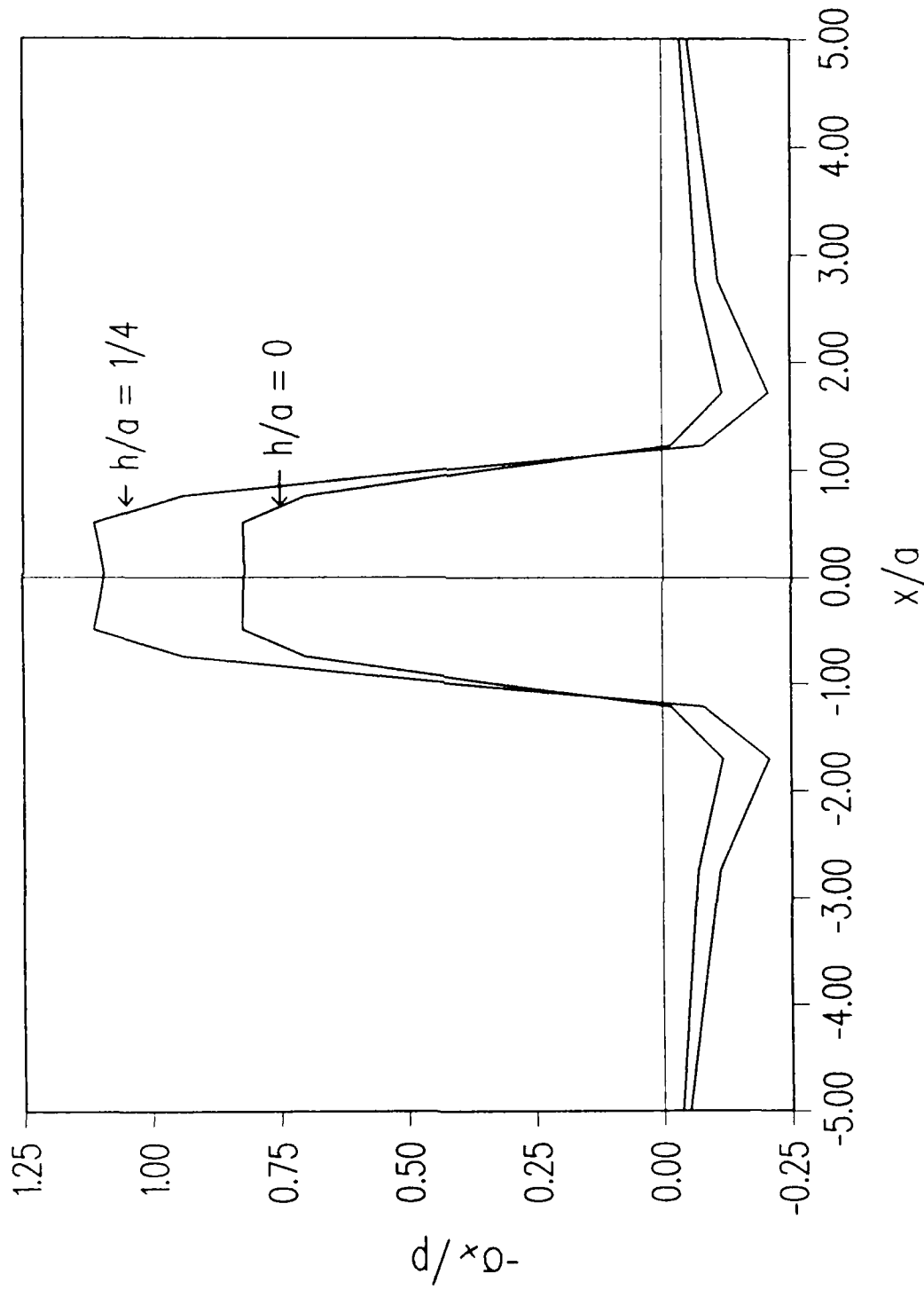


Figure 3-27. Subsurface coordinate stress,  $\sigma_x$ , under the rectangular load.

# X COORDINATE STRESS FOR 3-D MODEL



normal loading,  $b/a = 2, y = z = 0$

Figure 3-28. Variation of surface stress,  $\sigma_x$ , along the  $x$ -axis under a rectangular normal load compared for the cases of with and without coating.

# X COORDINATE STRESS FOR 3-D MODEL

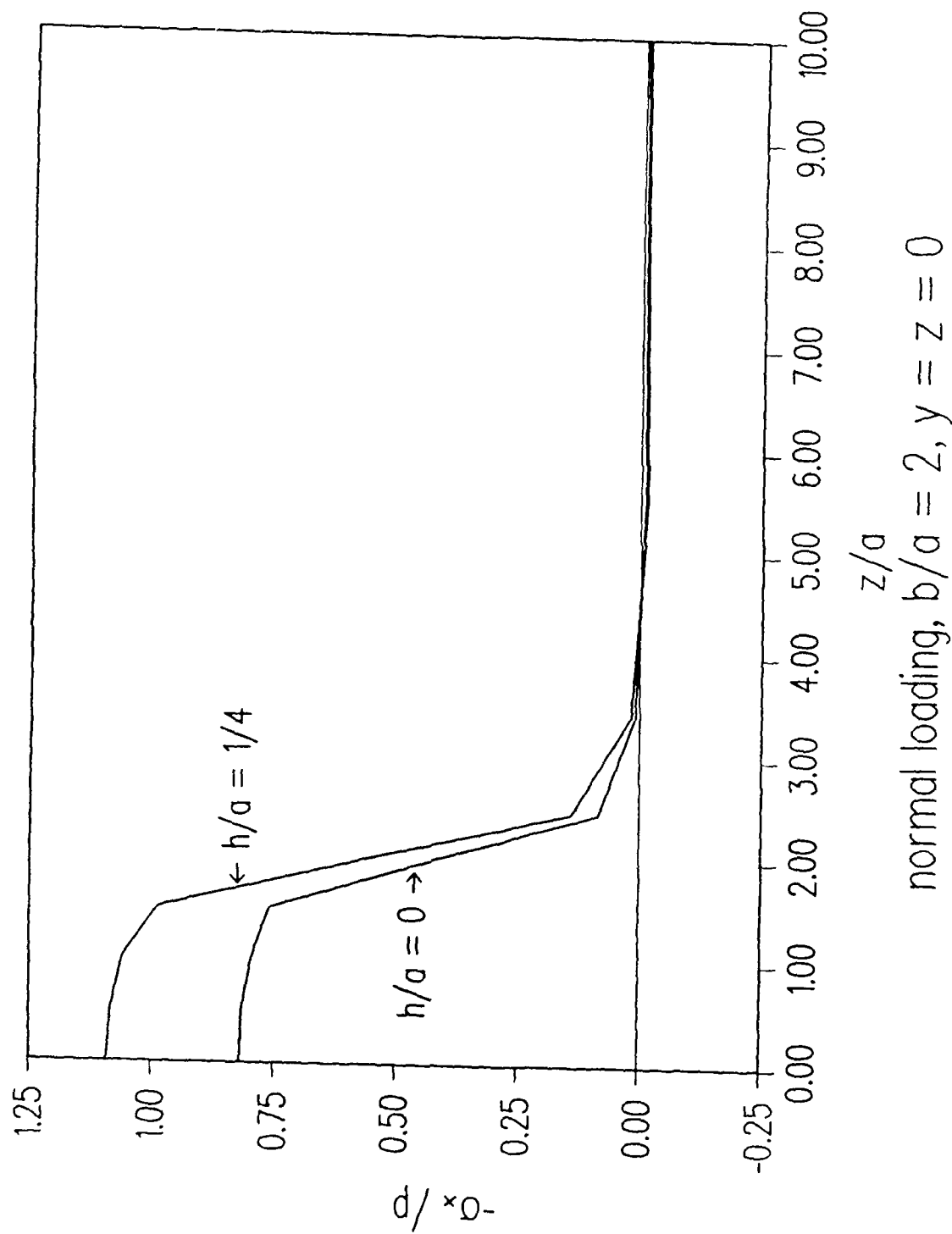


Figure 3-29 Variation of surface stress,  $\sigma_x$ , along the  $z$ -axis under a rectangular normal load compared for the cases of with and without coating.



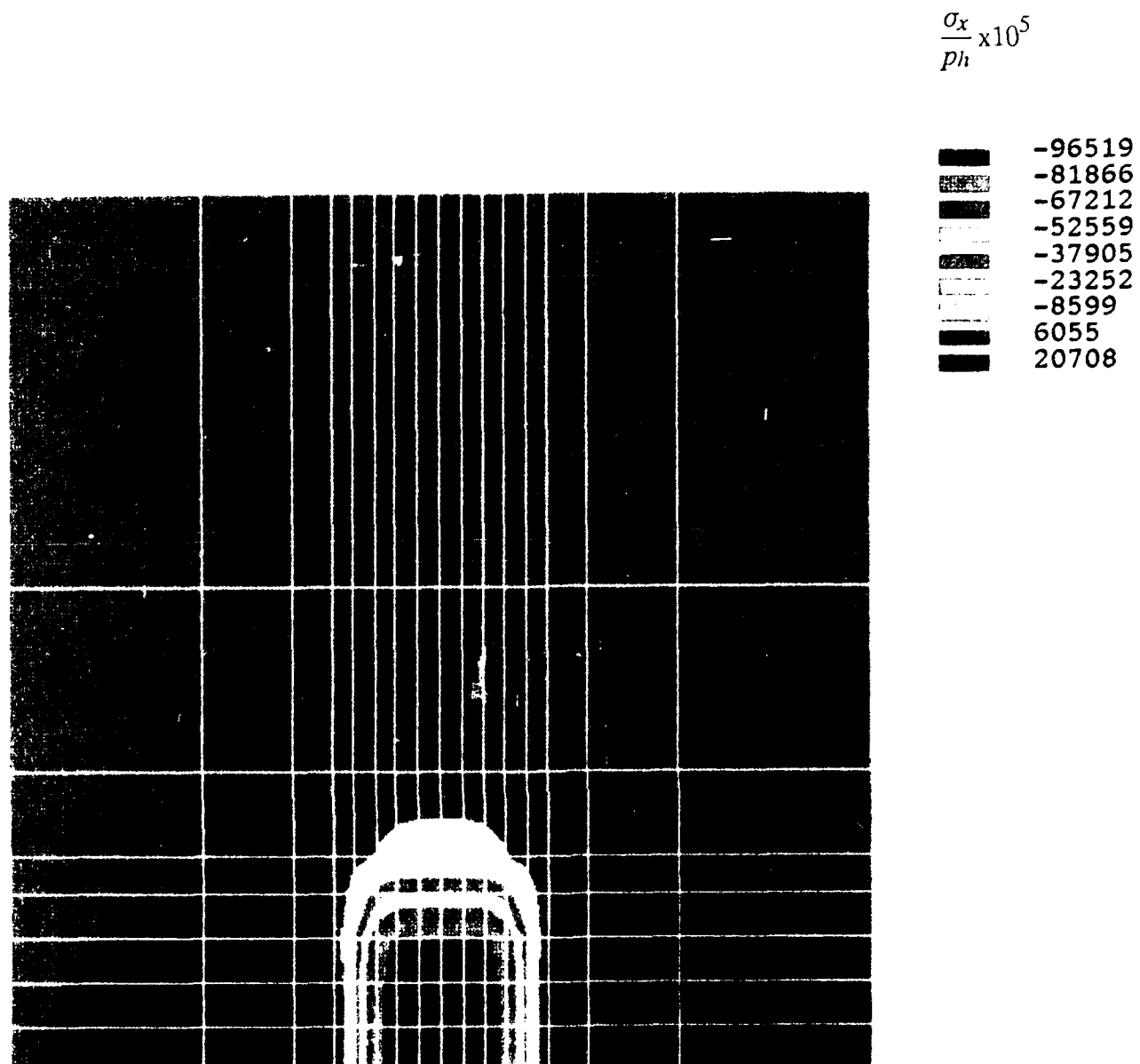


Figure 3-30. Contours of  $\sigma_x$  under a normal rectangular loading on the surface.

The above solutions clearly demonstrate the strength of the finite element approach to modeling a three-dimensional contact geometry. These solutions, when combined with the two-dimensional solutions and the validations against the solutions obtained by the Fourier transform approach, and those predicted by the classical Hertz theory, prove the feasibility of the modeling approach to the design of coated solids.

## 4. SUMMARY

The personal computer based PC-ANSYS finite element code is used to develop a finite element approach to model stresses in coated solids is considered. A plane-strain problem is first considered to prove technical feasibility of the approach. Parametric runs over several design parameters, such as coating thickness, materials properties and operating conditions, demonstrate the practical significance of the model. Extension of the plane strain model to the more complicated three-dimensional contact is demonstrated by modeling a rectangular contact area with uniform pressure. This preliminary three-dimensional model, along with the validated results of the two-dimensional model, clearly demonstrate the technical feasibility and practical design significance of the modeling approach. In addition, the preliminary models provide a strong technical foundation to develop more rigorous and sophisticated models for a wide range of practical applications.

The stress distributions in the coating and substrate are computed with the coated surface subjected to elliptically distributed normal and shear loadings under plane strain conditions. To model thermal loading, the temperature distribution in the entire solid, resulting from a prescribed heat flux on the coating surface, is first computed by a finite difference analysis; the computed temperatures are then input to the finite element model and the resulting thermal stresses are computed. In the absence of a coating, predictions of the finite element model are shown to agree with the classical Hertzian theory with a maximum of 1% deviation. With the coating present, a well established Fourier transform approach is used to validate the predictions of the finite element model. Once again, the deviation of the stress distributions obtained by both these models is shown to be less than 1%.

With an elliptically distributed heat flux on the coating surface, the thermal stresses in the entire solid are calculated to further establish the practical significance of the finite element model. In parallel, the Fourier transform approach is modified to permit an arbitrary displacement boundary condition at the coating/substrate interface to provide a preliminary model to simulate a thermal mismatch due to different thermal coefficient of expansion of the coating and substrate materials. Parametric runs as a function of coating thickness, and applied thermal and mechanical loadings demonstrate the practical significance of the models for materials selection, coating thickness optimization, and selection of coating application techniques and procedures to permit acceptable limiting shear and "break-away" stress limits in the coating and at the coating/substrate interface.

Validation of the three-dimensional model with a rectangular loading is tested by back calculating the boundary loading and comparing it with the applied conditions. Such comparisons are carried out both with and without a coating, and the results in both cases are quite encouraging.

For a three-dimensional contact, relevant to geometrically complicated interactions, the mass storage and computing speed requirements impose some restrictions on the use of personal computer systems and a demand for a more advanced computer work station or a mainframe computer system becomes clear. However, the results obtained with the PC-ANSYS system do prove technical feasibility of the overall approach and they provide a sound

analytical foundation for a more rigorous development in the future. In addition, the parametric results have some immediate significance for practical design of coated solids subjected to concentrated contact loads.

## 5. RECOMMENDATIONS FOR FUTURE DEVELOPMENT

Results of this Phase I investigation prove the technical feasibility and practical significance of the overall analytical approach to modeling of stresses in coated solids. The good agreement between the finite element approach, the numerical integral formulations, and the classical Hertz type solutions establishes the predictive strengths of the models. While the Fourier transform approach provides accurate numerical solutions to simplified contact configurations, the finite element models are applicable to arbitrary geometries, and they permit modeling of fairly complex mechanical and thermal loading. In practice, the process of materials selection and development consists of simple friction and wear tests where the coatings are applied to simple specimens with well defined geometry. Once the materials are proven in such test, the coatings are applied to real components, such as bearings, gears, piston rings or liners, and similar mechanical components. Thus it is essential to develop analytical modeling techniques for both simplified contact configurations and complicated contacts with complex geometries and loadings. Further advancement of both the numerical integral models and the finite element techniques is, therefore, essential. The following are some recommendations for further development.

1. The current plane strain integral model, and the computer program, LAYER, should be extended to treat multiple coatings. This will be extremely useful in modeling composite solids. Furthermore, by making the coating thickness small, an almost continued variation in properties through the solid can be modeled.

2. The plane strain model should be extended to treat any prescribed temperature field. In fact, a thermal model, similar to the one discussed in this report, should be incorporated in the plane strain integral model to automatically calculate the temperature field and the resulting thermal stresses in the solid.

3. The effort in the above two steps can be combined to model the effect of property variation as a function of temperature. Thus the net effect of both the thermal stresses due to the applied temperature field and the change in mechanical stresses due to altered fundamental properties can be simultaneously determined. Aside from designers, such a model will be valuable to be materials development scientists and chemists.

4. Experimental validation of analytical predictions is essential to enhance the design strengths of the models. Some of the available failure data may be used to validate the model for predictions of interfacial tensile and shear stresses.

5. Modeling of elliptical contacts is another extension of the current plane strain model. This can be a rather complex task because the current Fourier transforms have to be replaced with more complex Hankel transforms.

6. The finite element techniques can be easily advanced to model three-dimensional contacts. Perhaps, this approach may provide solutions to elliptical contacts fairly efficiently. It may be essential to develop these models on a main frame computer due to rather large mass storage and fast computing speed requirements.

7. For practical implementation of the finite element models, there are several areas which require development. Automatic mesh and load generators are essential for efficient problem definition. The finite element packages, such as NASTRAN and ANSYS, require an input data file, the preparation of which can become fairly tedious as the complexity of the problem increases. It is, therefore, essential to develop a "pre-preprocessor" to efficiently assemble the required input data files for the finite element models. Similarly, a "post-postprocessor" is sometimes essential to present the results in easily understandable engineering terms.

8. Once a large number of validated solutions are obtained by both finite element and the Fourier transform approaches, the results may be incorporated into a design data base. Basically, the results can be cataloged in terms of curve fits and systematic table lookups. Such a data base can be easily implemented on a personal computer and it can be an efficient tool for materials developers and practical designers.

9. In addition to the stress solutions, the practical significance of the above data base can be significantly enhanced by including the available materials property data. Such an enhancement provides fairly quick and efficient assessment of break-away stresses and identification of possible failures in a wide range of practical application.

10. The above design data base can also be interfaced with full finite element and numerical integral solutions. This permits easy modeling of problems which are beyond the limits of the data base.

## REFERENCES

1. Aleksandrov, V. M., "On the Approximate Solution of a Certain Type of Integral Equation", *Prikladnaya Matematika y Mekhanika*, vol 26, in English translation, pp 1410, 1962.
2. Aleksandrov, V. M., "Some Contact Problems of Elastic Layer", *Prikladnaya Matematika y Mekhanika*, vol 27, in English translation, pp 1164, 1963.
3. Aleksandrov, V. M., "Asymptotic Methods in Contact Problems in Elasticity Theory", *Prikladnaya Matematika y Mekhanika*, vol 32, in English translation, pp 691, 1968.
4. Aleksandrov, V. M., "Asymptotic Solution of the Contact Problem for a Thin Elastic Layer", *Prikladnaya Matematika y Mekhanika*, vol 33, in English translation, pp 49, 1969.
5. Meijers, P., "The Contact Problem of a Rigid Cylinder on an Elastic Layer", *Applied Scientific Research*, vol 18, pp 353, 1968.
6. Wu, T. and Chiu, Y. P., "On the Contact Problem of Layered Elastic Solids", *Quarterly of Applied Mathematics*, XXV, pp 233, 1967.
7. Pao, Y. C., Wu, T. and Chiu, Y. P., "Bounds on Maximum Contact Stress of an Indented Elastic Layer", *Journal of Applied Mechanics*, vol 38, No. 3, Trans ASME, vol 93E, pp 638, 1971.
8. Gupta, P. K. and Walowit, J. A., "Contact Stresses Between an Elastic Cylinder and a Layered Elastic Solid", *Journal of Lubrication Technology*, ASME Trans, vol 96F, No. 2, pp 250, 1974.
9. Lemcoe, M. M., "Stresses in Layered Elastic Solids", *Proc ASCE*, EM4, pp 1, August 1960.
10. Barovich, D., Kingsley, S. C. and Ku, T. C., "Stresses on a Thin Strip or Slab with Different Elastic Properties From That of the Substrate Due to Elliptically Distributed Load", *International Journal of Engineering Sciences*, vol 2, pp 253, 1964.
11. Ku, T. C., Kingsley, S. C. and Ramsey, H., "Stresses in a Thin Slab With Different Elastic Properties From That of the Substrate Due to Distributed Normal and Shearing Forces on the Surface of the Slab", *International Journal of Engineering Sciences*, vol 3, pp 93, 1965.
12. Gupta, P. K., Walowit, J. A. and Finkin, E. F., "Stress Distributions in Plane Strain Layered Elastic Solids Subjected to Arbitrary Boundary Loading", *Journal of Lubrication Technology*, ASME Trans, vol 95F, pp 427, 1973.
13. Gupta, P. K., *LAYER - A Computer Code for Analysis of Plane-Strain Layered Elastic Solids*, PKG Inc, 1984.

14. Gupta, P.K., ADVANCED DYNAMICS OF ROLLING ELEMENT, Springer-Verlag, 1984.



## APPENDIX

### Thermal Analysis of Semi-infinite Solid with a Moving Heat Source

Consider the contact geometry shown schematically in figure A-1. The solid may either consist of multiple coatings with different properties, or the properties may have a continuous variation with the depth coordinate  $y$ . The conduction equation is written as:

$$\rho c u \frac{\partial T}{\partial x} = \frac{\partial}{\partial y} \left( K \frac{\partial T}{\partial y} \right) + K \frac{\partial^2 T}{\partial x^2} \quad (\text{A-1})$$

with the distant boundary condition

$$\lim_{|x|, |y| \rightarrow \infty} \tilde{T} = 0 \quad (\text{A-2})$$

For convenience, introduce the following dimensionless quantities:

$$\tilde{\rho} = \frac{\rho}{\rho_s}, \quad \tilde{c} = \frac{c}{c_s}, \quad \tilde{K} = \frac{K}{K_s}, \quad \tilde{x} = \frac{x}{a}, \quad \eta = \left[ \frac{\rho_s c_s u}{K_s a} \right]^{1/2} y$$

where  $K, \rho, c$  denote thermal conductivity, density and specific heat respectively. The subscript,  $s$ , denotes the substrate for a coated solid, or in general, it can represent the base properties at any characteristic reference point. In fact, the base properties may be chosen such that the dimensionless quantities,  $K, \rho, c$ , are of order 1. The characteristic length,  $a$ , is taken as the contact half width of the region of input flux, as shown in figure A-1.

With the above definitions, equation (A-1) is now written as:

$$\tilde{\rho} \tilde{c} \frac{\partial T}{\partial \tilde{x}} = \frac{\partial}{\partial \eta} \left( \tilde{K} \frac{\partial T}{\partial \eta} \right) + \frac{\tilde{K}}{P} \frac{\partial^2 T}{\partial \tilde{x}^2} \quad (\text{A-3})$$

where  $P = \frac{u \rho_s c_s a}{K_s}$ , is the Peclet number. For prescribed properties, it really is proportional to speed. Under the conditions of high-speed rolling/sliding contact, such as the ones encountered in high-speed rolling bearings, the Peclet number is generally very high. As an example, for steel, the volumetric specific heat  $\rho c = 1.10 \times 10^6 \text{ N/M}^2/^{\circ}\text{C}$ , and the thermal conductivity, and the contact half width for a typical 30 mm bore roller bearing operating at a moderate speed of 35,000 rpm, may be 40 M/Sec and  $4.0 \times 10^{-5} \text{ M}$  respectively. These values result in a Peclet number of about 120. Thus for many applications of concentrated contacts, a high

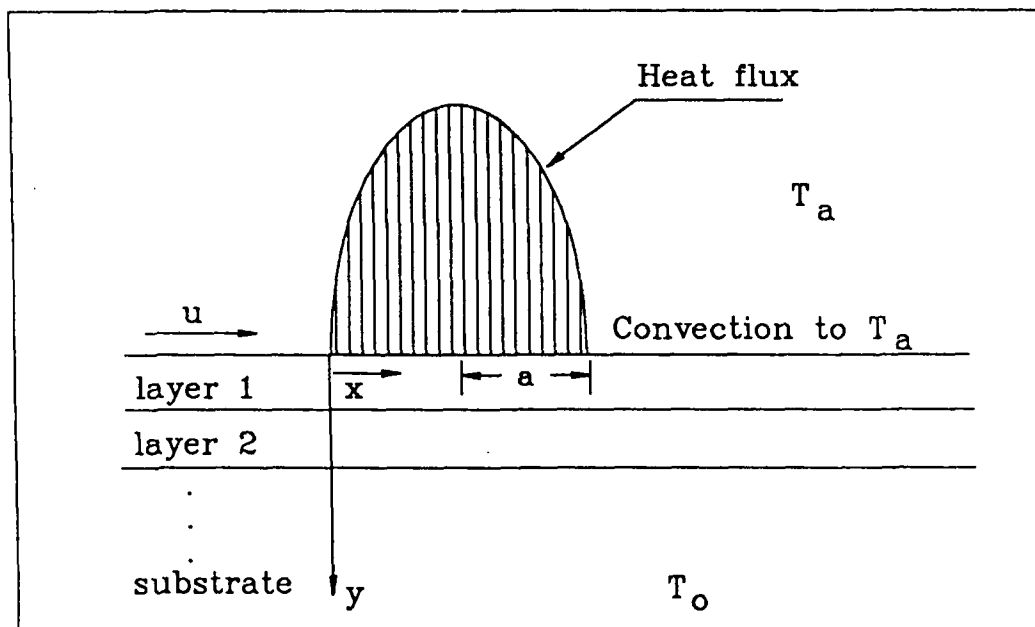


Figure A-1. Coordinate schematic for the thermal model.

Peclet number approximation is quite reasonable. Thus, the last term in equation (A-3) may be dropped and the conduction equation may be written as:

$$P \tilde{\rho} \tilde{c} \frac{\partial \tilde{T}}{\partial x} = \frac{\partial}{\partial y} \left( \tilde{K} \frac{\partial \tilde{T}}{\partial y} \right), \quad \tilde{x}, \tilde{y} > 0 \quad (\text{A-4})$$

with the boundary conditions

$$\tilde{T} = 0 \text{ at } \tilde{x}=0, \text{ and } \lim_{\tilde{y} \rightarrow \infty} \tilde{T} = 0 \quad (\text{A-5})$$

where  $\tilde{y} = y/a$ ,  $a$  being the half width of contact.

If  $q_o$  is the amplitude of input flux, the flux distribution in the contact may be written as

$$q = q_o f(\tilde{x}) \quad (\text{A-6})$$

and the surface input flux condition is written as

$$-\tilde{K} \frac{\partial \tilde{T}}{\partial y} = f(\tilde{x}), \quad \text{at } y=0 \text{ and } 0 \leq \tilde{x} \leq 2 \quad (\text{A-7})$$

where  $\tilde{T} = \frac{T - T_r}{T_r}$ , with  $T_r = \frac{q_o a}{K_s}$  as a reference temperature.

The convective heat transfer condition is

$$-\tilde{K} \frac{\partial \tilde{T}}{\partial y} = \tilde{H} (\tilde{T} - \tilde{T}_a), \quad \text{at } y=0 \text{ and } \tilde{x} > 2 \quad (\text{A-8})$$

where  $\tilde{T}_a$  is the dimensionless ambient temperature  $\frac{T_a}{T_r}$ , and  $\tilde{H} = \frac{h a}{K_s}$  is the Nusselt number with a heat transfer coefficient  $h$ .

For most concentrated contacts it may be reasonable to assume that the heat flux is proportional to the contact pressure. Thus the heat flux function in equation (A-6) may be written as

$$f(\tilde{x}) = \left[ 1 - (\tilde{x} - 1)^2 \right]^{1/2}, \quad 0 \leq \tilde{x} \leq 2 \quad (\text{A-9})$$

For any arbitrary variation in properties, the above equations are best solved numerically by finite difference approximations. A grid structure, shown schematically in figure A-2, is chosen starting at  $x = y = 0$ . For brevity, the  $\tilde{\cdot}$  is dropped in all the following formulation for numerical analysis.

For performing heat flow balance over the dotted rectangle, as shown in figure A-2, the heat flow out of the rectangle across the surface c is written as

$$-K_i \left[ \frac{1}{2} \left( \frac{T_{j,i+1} - T_{j,i}}{\Delta y_i} \right) + \frac{1}{2} \left( \frac{T_{j+1,i+1} - T_{j+1,i}}{\Delta y_i} \right) \right] \Delta x_j$$

and the heat flow out of the rectangle across surface b is written as

$$P \left[ \frac{1}{2} \rho_{i-1} c_{i-1} T_{j+1,i-1} + \frac{1}{2} \rho_{i-1} c_{i-1} T_{j+1,i} \Delta y_i \right]$$

In the above expressions  $\Delta x_j = x_{j+1} - x_j$  and  $\Delta y_i = y_{i+1} - y_i$ ; and, the properties,  $K_i, \rho_i, c_i$  prevail in the interval  $y_i \leq y \leq y_{i+1}$ .

Using the above relations, the flow across all four sides of the rectangle may be written and the sum may be equated to zero to derive the following equation:

$$\begin{aligned} & P (T_{j,i} - T_{j+1,i}) (\rho_{i-1} c_{i-1} \Delta y_{i-1} + \rho c_i \Delta y_i) + \\ & K_i (T_{j,i+1} - T_{j,i} + T_{j+1,i+1} - T_{j+1,i}) \frac{\Delta x_j}{\Delta y_i} - \\ & K_{i-1} (T_{j,i} - T_{j,i-1} + T_{j+1,i} - T_{j+1,i-1}) \frac{\Delta x_j}{\Delta y_{i-1}} = 0 \end{aligned} \quad (\text{A-10})$$

The above equation applies to the interior points defined by  $j > 1, 1 < i < m$ , where  $m$  is the total number of points in the  $y$  direction. Also, the boundary condition at  $y = \infty$  is applied at  $y = y_m$ .

The boundary conditions at  $x=0$  and at  $y=y_m$  result in the following boundary values

$$T_{1,j} = 0 \text{ and } T_{j,m} = 0 \quad (\text{A-11})$$

Similar heat flow balances may be obtained over the "half" rectangles bounding the surface with flux inputs corresponding to equations (A-7) and (A-8). The resulting equation

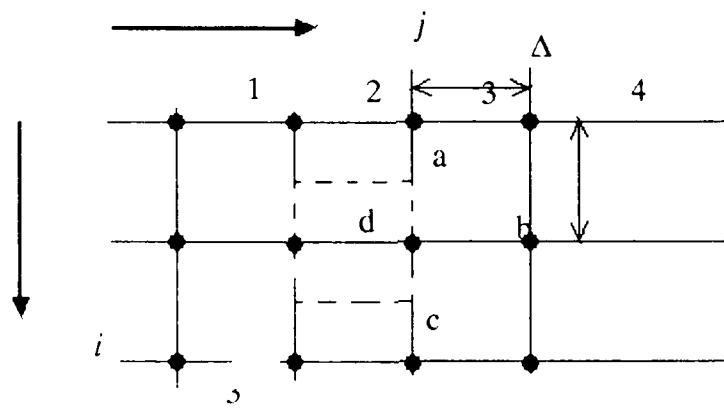


Figure A-2. Numerical grid structure for the finite difference computation.

at  $i = 1, j > 1$  is written as

$$P \rho_i c_i (T_{j,i} - T_{j+1,i}) + (f_j + f_{j+1}) \Delta x_j - H (T_{j,i} + T_{j+1,i} - 2 T_a) \Delta x_j + K_i (T_{j,i+1} - T_{j,i} + T_{j+1,i+1} - T_{j+1,i}) \frac{\Delta x_j}{\Delta y_i} = 0 \quad (\text{A-12})$$

Equations (A-10) to (A-12) when used to solve for  $T_{j+1,i}$  represent a modified Crank-Nicholsen approach which is generally stable and provides quadratic accuracy. The equations for any column  $j$  may be written in the form

$$C_i T_{j,i} + D_i T_{j,i+1} + \epsilon_i T_{j,i-1} = R_i \quad (\text{A-13})$$

where  $R_i$  depends on  $T_{j-1,i}$ , which is obtained from equation (A-11) for  $j=1$  and the previous solution to equation (A-13) for  $j>1$ . The remaining coefficients are independent of temperature.

If we look for a solution in the form

$$T_{j,i-1} = A_i T_{j,i} + B_i \quad (\text{A-14})$$

then by substituting  $T_{j,i-1}$  in equation (A-13) and solving for  $T_{j,i}$  we obtain

$$T_{j,i} = A_{i+1} T_{j,i+1} + B_{i+1} \quad (\text{A-15})$$

where

$$A_{i+1} = -\frac{D_i}{C_i + \epsilon_i A_i} \quad (\text{A-16})$$

and

$$B_{i+1} = \frac{R_i - \epsilon_i B_i}{C_i + \epsilon_i A_i} \quad (\text{A-17})$$

Since the temperatures start at  $i=1$  we can take  $A_1 = B_1 = 0$ , then use equations (A-16) and (A-17) to calculate all  $A$  and  $B$  values up to  $A_m$  and  $B_m$ . From equation (A-11)  $T_{j,m} = 0$ ,

hence, equation (A-14) may be used to calculate the remaining temperatures from  $T_{j,m-1}$  to  $T_{j,1}$ . The procedure is then repeated for the next column until the required temperature map is obtained.

The above method of solution for the temperatures in a given column implements a Riccati transformation which provides good numerical accuracy even for relatively long spans in the  $y$  coordinate.

In the event the properties are assumed to be constant and the convection term is neglected, the solution may be written in terms of an integral. This is accomplished by substituting  $K = \tilde{\rho} = c = 1$  and  $H = 0$  and by solving equations (A-4) to (A-7) by Laplace transforms. The temperature distribution as a function of the input flux is written as

$$\tilde{T}(\tilde{x}, 0) = \frac{1}{\sqrt{\pi}P} \int_0^{\tilde{x}} \frac{f(\tilde{x}')}{(\tilde{x} - \tilde{x}')^{1/2}} d\tilde{x}' \quad (\text{A-18})$$

The above relation may be readily used to check out the numerical results when implementing the above general procedure in a computer code. Also, the above relation suggests using an effective temperature

$$T^* = \frac{T_r}{\sqrt{\pi}P}$$

as a characteristic dimensional parameter for temperatures.